Supplementary Materials for

Customization of Cloud Temperature in Amphiphilic π-Systems by Photoisomerization and Supramolecular Co-assembly for Smart Window Application

Dipak Patra[a,b] and Ayyappanpillai Ajayaghosh* [a,b,c]

[a] Dr. D. Patra, and Prof. Dr. A. Ajayaghosh

Chemical Sciences and Technology Division,

CSIR-National Institute for Interdisciplinary Sciences and Technology (CSIR-NIIST),

Thiruvananthapuram 695019, India

[b] Dr. D. Patra, and Prof. Dr. A. Ajayaghosh

Academy of Scientific and Innovative Research (AcSIR)

Ghaziabad-201002, India

[c] Prof. Dr. A. Ajayaghosh

SRM Institute of Science and Technology, Kattankulathur, Chennai 603203, India

E-mail: ajayagha@srmist.edu.in

Supporting information

1. Experimental Details: Instrumental Procedures

NMR experiments:

^{1}H NMR, and ^{13}C NMR recorded on proton (500 MHz) and carbon NMR (125 MHz) spectra recorded on a 500 MHz Bruker Avance DPX spectrometer. Chemical shifts reported in parts per million (ppm) using tetramethylsilane (TMS) (δ_H = 0 ppm) or the solvent residual signal ($CDCl_3$: δ_C = 77.00 ppm and CD_3CN: δ_C = 118.00 ppm as internal references. The obtained experimental data processed using MestReNova software. The resonance multiplicity described as s (singlet), d (doublet), t (triplet), and m (multiplet).

High-Resolution Mass Spectrometry (HRMS):

High-resolution mass spectra recorded using Thermo Scientific Q ExactiveOrbitrap electrospray ionization mass spectrometer.

Fourier transform infrared spectroscopy (FT-IR):

Fourier transform infrared (FT-IR) spectra performed in Perkin-Elmer-Spectrum using Attenuated total reflectance (ATR) techniques by pressing the sample towards an ATR crystal (e.g., diamond).

UV-Vis experiment:

Variable-temperature electronic absorption spectra recorded on a Shimadzu UV-2600 Spectrophotometer equipped with a Peltier thermostatic cell holder for cooling and heating rate at 2 °C/ min.

Dynamic Light Scattering (DLS):

DLS analyses conducted with a Zetasizer Nano S from Malvern Instruments at 25 °C. The average hydrodynamic radii calculated from the Stork-Einstein equation ($R_H=K_BT/(6\pi\eta D)$. 'D' is the translational diffusion coefficient [m^2/s]. K_B = Boltzmann constant [m^2kg/Ks^2], T= Temperature [K], η = viscosity [Pa.s], R_H = Hydrodynamic radius [m]. For LCST Studies, the solution then kept in the cold-water bath (< 20 °C) and gently shaken to ensure homogeneity. The aqueous solution is sealed and kept at a temperature < 25 °C.

High Resolution Transmission Electron Microscopy (HR-TEM):

HR-TEM images were performed on a JEOL JEM F200 microscope with an accelerating voltage of 100 kV. The samples were prepared by drop casting over a carbon coated copper grid. TEM images were obtained without staining.

Transmittance (UV-Vis-NIR) study:

The transmittance spectra were carried out with a Lamda 950 UV-Vis-NIR spectrophotometer (PerkinElmer, USA) with an integrating sphere. The spectrophotometer was connected to thermostatically with a heating and cooling stage for variable-temperature studies.

2. Synthesis procedures and characterization

All reagents and solvents were sourced from commercial suppliers (Sigma Aldrich, Alfa Aesar, Merck, and TCI) and used without additional purification. Reactions sensitive to moisture and oxygen were carried out in a dry argon or nitrogen atmosphere. Organic extracts were dried using sodium sulfate (Na_2SO_4) powder, and solvents were removed under reduced pressure with a BUCHI R-210 rotary evaporator. Necessary solvents were distilled following standard literature procedures and maintained in an anhydrous environment. K_2CO_3 was activated by heating at 400 °C for four hours prior to use in reactions. Column chromatography utilized silica gel with a mesh size of 100-200, while thin layer chromatography was performed on neutral TLC aluminium oxide 60 F_{254} plates from Merck. HPLC-grade solvents were employed for precipitation and optical studies.

Synthesis of ANT and PYR

ANT(Z) and **PYR(Z)** were synthesized according to the following procedure.[1, 2]

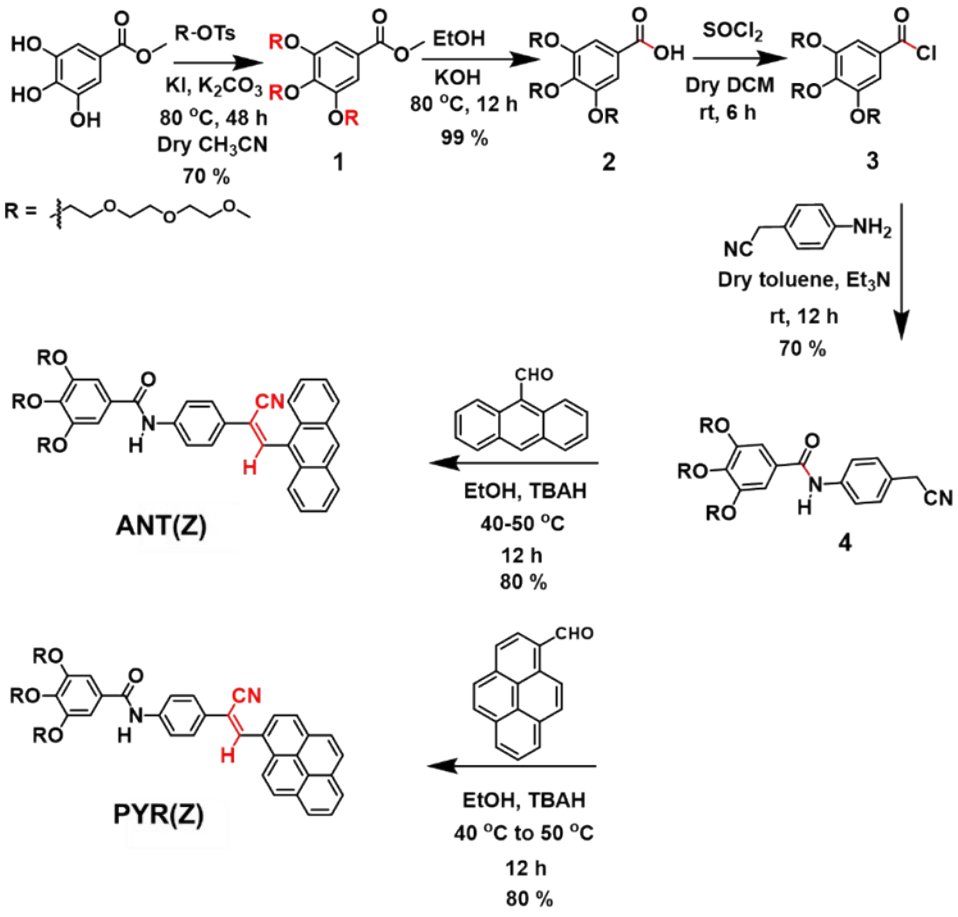

Scheme: S1. Synthesis of **ANT(Z) and PYR(Z).**

Synthesis of ANT(Z):

Under an atmosphere of nitrogen, Compound **4** (0.300 g, 0.416 mmol), and anthracene-9-carbaldehyde (0.086 g, 0.416 mmol) were added in a 100 ml round-bottom flask containing dry ethanol. The reaction mixture was stirred at room temperature for 30 min. After that, tert-butylammonium hydroxide was added through a syringe. The solution was stirred at 50 °C for 12 h. After cooling to room temperature, the solvent evaporated under reduced pressure. The crude product was extracted using chloroform, washed with water, and brine, and dried over anhydrous sodium sulfate. The solvent evaporated under reduced pressure and the residue purified through silica gel column chromatography, using (5 % $CH_3OH/CHCl_3$) mixture as a pale-yellow liquid (**ANT(Z)**). Yield: 0.300 g, 80 %.

^{1}H NMR (500 MHz, CD_3CN): δ = 8.98 (s, 1H), 8.68 (s, 1H), 8.61 (s, 1H), 8.17-8.16 (m, 4H), 7.98 (d, J = 10 Hz, 2H), 7.95 (d, J = 10 Hz, 2H), 7.61-7.59 (m, 4H), 7.29 (s, 2H), 4.26-4.24 (m, 4H), 4.21-4.19 (m, 2H), 3.86-3.85 (m, 4H), 3.79-3.77 (m, 2H), 3.69-3.68 (m, 4H), 3.65-3.64 (m, 2H), 3.62-3.61 (m, 4H), 3.59-3.56 (m, 8H), 3.50-3.47 (m, 6H), 3.32 (s, 3H), 3.31 (s, 6H) ppm.

^{13}C NMR (125 MHz, CD_3CN): δ = 165.83, 153.09, 141.79, 140.12, 140.17, 131.83, 129.47, 127.34, 127.26, 126.31, 125.91, 121.28, 107.37, 72.88, 72.22, 72.20, 71.01, 70.97, 70.82, 70.80, 70.77, 70.62, 69.95, 69.43, 58.48 ppm.

HRMS (ESI): Molecular formula ($C_{51}H_{62}N_2O_{13}$), m/z, Calcd for $[M]^+$ 910.4252, found 911.4356 $[M+H]^+$, 933.4173 $[M+Na]^+$.

Synthesis of PYR(Z):

Under an atmosphere of nitrogen, Compound **4** (0.300 g, 0.416 mmol), and pyrene-1-carbaldehyde (0.096 g, 0.416 mmol) were added in a 100 ml round-bottom flask containing dry ethanol. The reaction mixture was stirred at room temperature for 30 min. After that, tert-butylammonium hydroxide was added through a syringe. The solution was stirred at 50 °C for 12 h. After cooling to room temperature, the solvent evaporated under reduced pressure. The crude product was extracted using chloroform, washed with water, and brine, and dried over anhydrous sodium sulfate. The solvent evaporated under reduced pressure and the residue was purified through silica gel column chromatography using (5 % $CH_3OH/CHCl_3$) mixture as a yellow liquid (**PYR(Z)**). Yield: 0.310 g, 80 %

^{1}H NMR (500 MHz, CD_3CN): δ = 8.93 (s, 1H), 8.60 (s, 1H), 8.525 (d, J = 5 Hz, 1H), 8.32 (d, J = 10 Hz, 1H), 8.29-8.26 (m, 3H), 8.19-8.16 (m, 2H), 8.115 (d, J = 5 Hz, 1H), 8.09-8.06 (t, J = 7.5 Hz, 1H), 7.92 (d, J = 10 Hz, 2H), 7.86 (d, J = 10 Hz, 2H), 7.24 (s, 2H), 4.21-4.16 (m, 6H), 3.82-3.76 (m, 6H), 3.66-3.63 (m, 6H), 3.60-3.57 (m, 12H), 3.50-3.48 (m, 6H), 3.32 (s, 3H), 3.30 (s, 6H) ppm.

^{13}C NMR (125 MHz, CD_3CN): δ = 165.77, 153.07, 140.03, 133.08, 129.16, 129.07, 127.90, 127.30, 127.16, 126.75, 126.72, 126.58, 125.32, 123.75, 121.24, 107.43, 72.23, 71.00, 70.82, 70.64, 69.98, 69.45, 58.51 ppm.

HRMS (ESI): Molecular formula ($C_{53}H_{62}N_2O_{13}$), m/z, Calcd. for $[M]^+$ 934.4352, found 935.4341 $[M+H]^+$, 957.4154 $[M+Na]^+$.

3. Experimental procedures

Protocol for sample preparation:

To perform spectroscopic experiments, spectroscopy-grade solvents are used. The stock solutions of **ANT** and **PYR** (10^{-2} M) are prepared in milli-Q water at high concentrations and used for all spectroscopy studies.

Protocol for ANT/PYR (1:1) (10^{-3} M) sample preparation:

For co-assembly studies, 0.5 mL aqueous solution of **ANT** (10^{-3} M) and 0.5 mL aqueous solution of **PYR** (10^{-3} M) are mixed up to prepare 1 mL of **ANT**/**PYR** (1:1) (10^{-3} M) aqueous solution. We have also prepared different ratios of 10^{-3} M **ANT**/**PYR** aqueous solutions (0.8:0.2, 0.6:0.4, 0.4:0.6, 0.2:0.8) by ratiometric mixing of **ANT** and **PYR**.

Protocol for Fourier transform infrared spectroscopy (FT-IR) studies:

The FT-IR spectra were recorded and analysed according to following literature procedure.[3] All samples were recorded in $CDCl_3$ (monomer state). The spectra were recorded in water for the aggregated state after freeze-drying from water.

Protocol for *Z/E*-photoisomerization and thermal back isomerization in aqueous medium:

Z/E-photoisomerization of **ANT(Z)** and **PYR(Z)** were studied by UV-vis absorption. An aqueous solution of **ANT(Z)** and **PYR(Z)** (5×10^{-5} M, milli-Q water, deoxygenated) was prepared and photoirradiated with 370 nm LED light used for *Z/E*-photoisomerization. Kinetic studies of thermal back isomerization were studied by variable-temperature UV-vis absorption spectroscopy in aqueous medium. Aqueous solutions of **ANT(Z)** and **PYR(Z)** (5×10^{-5} M) were irradiated at 365 nm light for *Z/E*-photoisomerization and then left the solution at a specific temperature. UV-vis absorption spectra were acquired at different time intervals to check the peak intensity as a function of time. The rate constants at different temperatures in aqueous medium were used to plot Arrhenius and Eyring fitting curves, from which the activation energy and all thermodynamic parameters were calculated to extrapolate the thermal half-lives at room temperature.

Protocol for *Z/E*-isomer ratios at the photostationary state (PSS) in water:

The *Z/E*-isomer ratios were calculated according to a literature procedure.[4] *Z/E*-isomer ratios at PSS were obtained by UV-Vis absorption spectroscopy. The isomer ratios at PSS were calculated using following equation:

$$\chi_Z = \frac{A_{PSS}}{A_0}$$

χ_Z Z-isomer ratio at PSS

A_0 Absorbance at initial state at λ_{max}

A_{PSS} Absorbance at PSS at λ_{max}

Protocol for device fabrication and combinatorial approach:

For the preparation of 10 cm × 10 cm glass window prototypes, the set-up consists of two glass plates, each of size 10 cm × 10 cm and thickness of 1.4 mm. The glass plates were sealed with an internal spacing of 1.4 mm. Aqueous solutions of **ANT**, **PYR**, and **ANT**/**PYR** (1:1) (10 mL, 1 mM) were injected into the system and sealed using UV-epoxy resin properly. For the combinatorial approach, four different types of smart window panels using **ANT**, **ANT**/**PYR** (1:1), **PYR**, and their combinations, namely **A**, **B**, **C**, and **D** respectively, were fabricated. Windows are arranged according to their different modules of **ANT**, **PYR,** and **ANT**/**PYR** (1:1) combinations.

Protocol for variable-temperature kinetic studies:

Variable-temperature transmittance studies during heating and cooling cycles were performed using a 1 mM quartz cuvette at a rate of 2 °C/min for all samples. During the heating and cooling process, a 10 × 10 cm^2 window prototype containing a freshly prepared aqueous solution of **ANT** underwent a phase transition from a transparent state at 24 °C to an opaque state at 27 °C and then returned to a transparent state when cooled back to 24 °C. To perform the thermal stability test, a 3 mL aqueous solution of **ANT** (1 mM) was taken from the window prototype. This aqueous solution was then transferred into a 1 cm quartz cuvette. Then, we performed variable-temperature transmittance kinetic studies for multiple heating and cooling cycles at a rate of 2 °C/min at 500 nm using a Shimadzu UV-2600 Spectrophotometer equipped with a Peltier thermostatic cell holder. The measurements were performed with the same solution for every 1000 consecutive heating and cooling cycles for 10 times. We followed the same experimental procedures for **PYR** and **ANT**/**PYR** (1:1) for multiple heating and cooling cycles. We have calculated the response time for the heating and cooling process from these UV-Vis kinetic spectra.

Protocol for Transmittance (UV-Vis-NIR) studies:

The solar transmittance (T_{solar}), luminous transmittance (T_{lum}), and IR transmittance (T_{IR}) were calculated using literature procedures.[5-7] The transmittance spectra were recorded with a Lamda 950 UV-Vis-NIR spectrophotometer (PerkinElmer, USA) with an integrating sphere attached. The calculation of integral solar transmittance (400-2500 nm), luminous transmittance (400-780 nm), IR transmittance (780-2500 nm) and the corresponding transmittance modulations (ΔT_{solar}, ΔT_{lum}, ΔT_{IR}) were obtained by Equations 1 and 2, respectively.

Equation 1: $$T_{lum/IR/solar} = \frac{\int \varphi_{lum/IR/solar}(\lambda) T(\lambda) d\lambda}{\int \varphi_{lum/IR/solar}(\lambda) d\lambda}$$

Equation 2: $$\Delta T_{lum/IR/solar} = T_{lum/IR/solar}(\text{at temperature} \leq T_{cloud}) - T_{lum/IR/solar}(\text{at temperature} \geq T_{cloud})$$

where $T(\lambda)$ is the recorded transmittance spectra at a particular wavelength, "φ_{lum}" is the standard luminous efficiency function for the photopic vision of the human eye.

4. Supporting Figures and Tables

(a) (b)

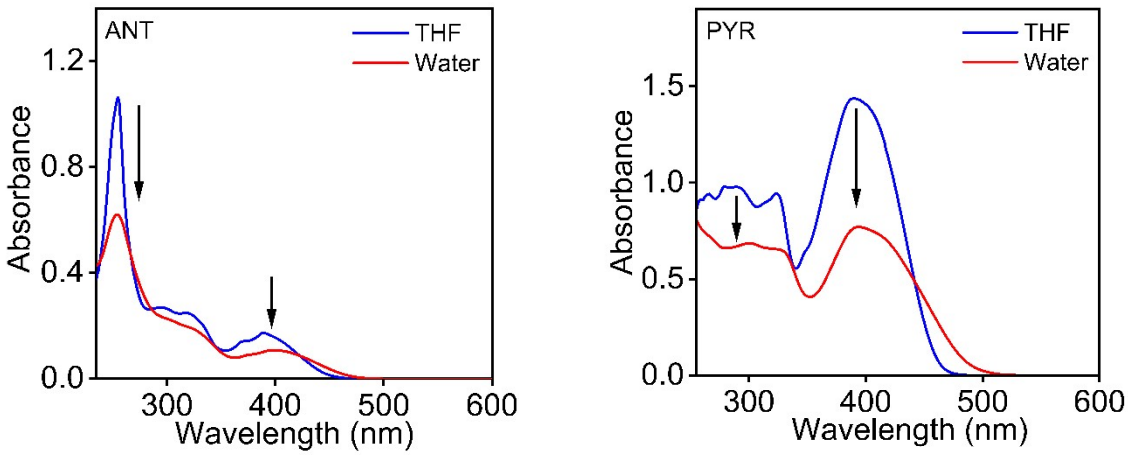

Figure S1. UV-Vis absorption spectra of **ANT** and **PYR** in THF and aqueous medium.

(a) (b) (c)

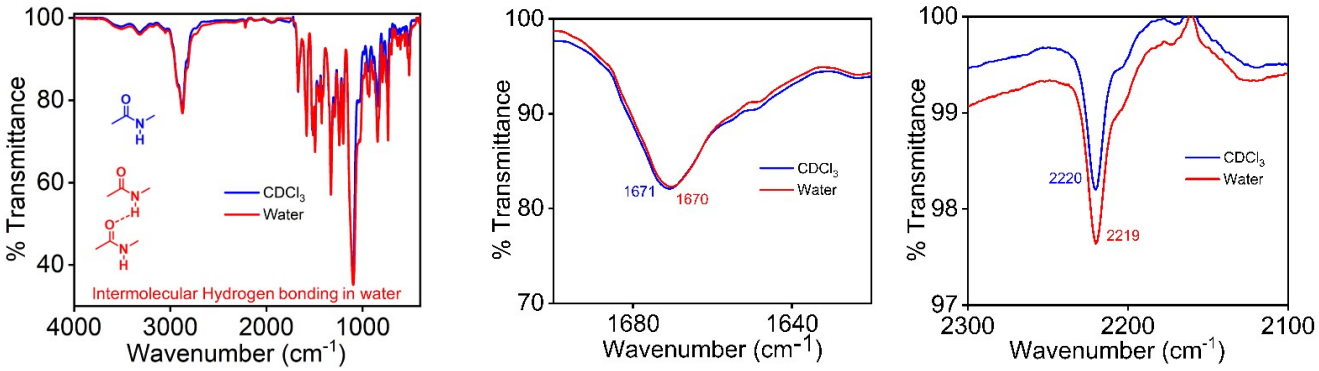

Figure S2. (a) FT-IR spectra of **ANT(Z)** in $CDCl_3$ (blue line) and water (red line) medium. (b) The sharp amide I band shifted from 1671 cm^{-1} in $CDCl_3$ (monomers) to 1670 cm^{-1} in H_2O (aggregation), suggesting the presence of intermolecular hydrogen-bond between the amide N-H bond. (c) The sharp -CN band shifted from 2220 cm^{-1} to 2219 cm^{-1}, suggesting [CN…H] interactions in aqueous medium.

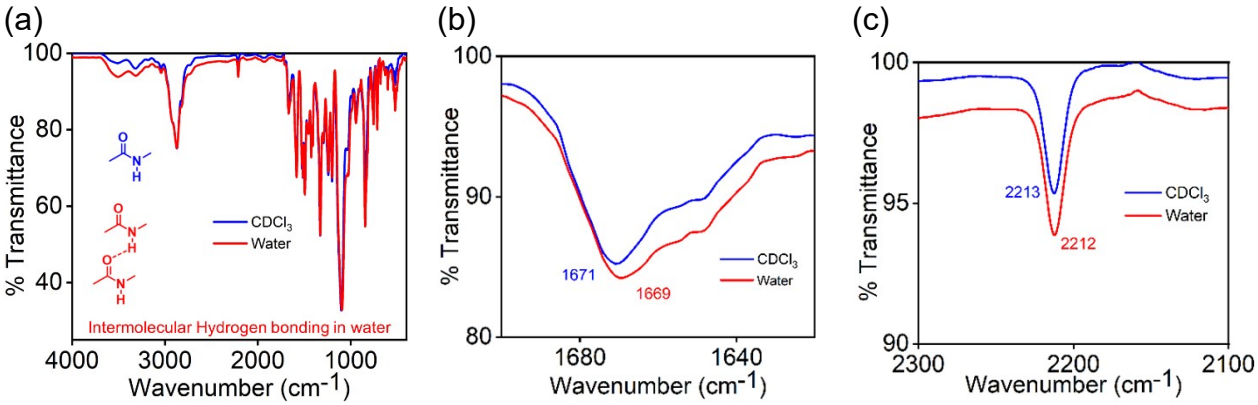

Figure S3. (a) FT-IR spectra of **PYR(Z)** in $CDCl_3$ (blue line) and water (red line) medium. (b) (b) The sharp amide I band shifted from 1671 cm^{-1} in $CDCl_3$ (monomers) to 1669 cm^{-1} in H_2O (aggregation), suggesting the presence of intermolecular hydrogen-bond between the amide N-H bond. (c) The sharp -CN band shifted from 2213 cm^{-1} to 2212 cm^{-1}, suggesting [CN…H] interactions in aqueous medium.

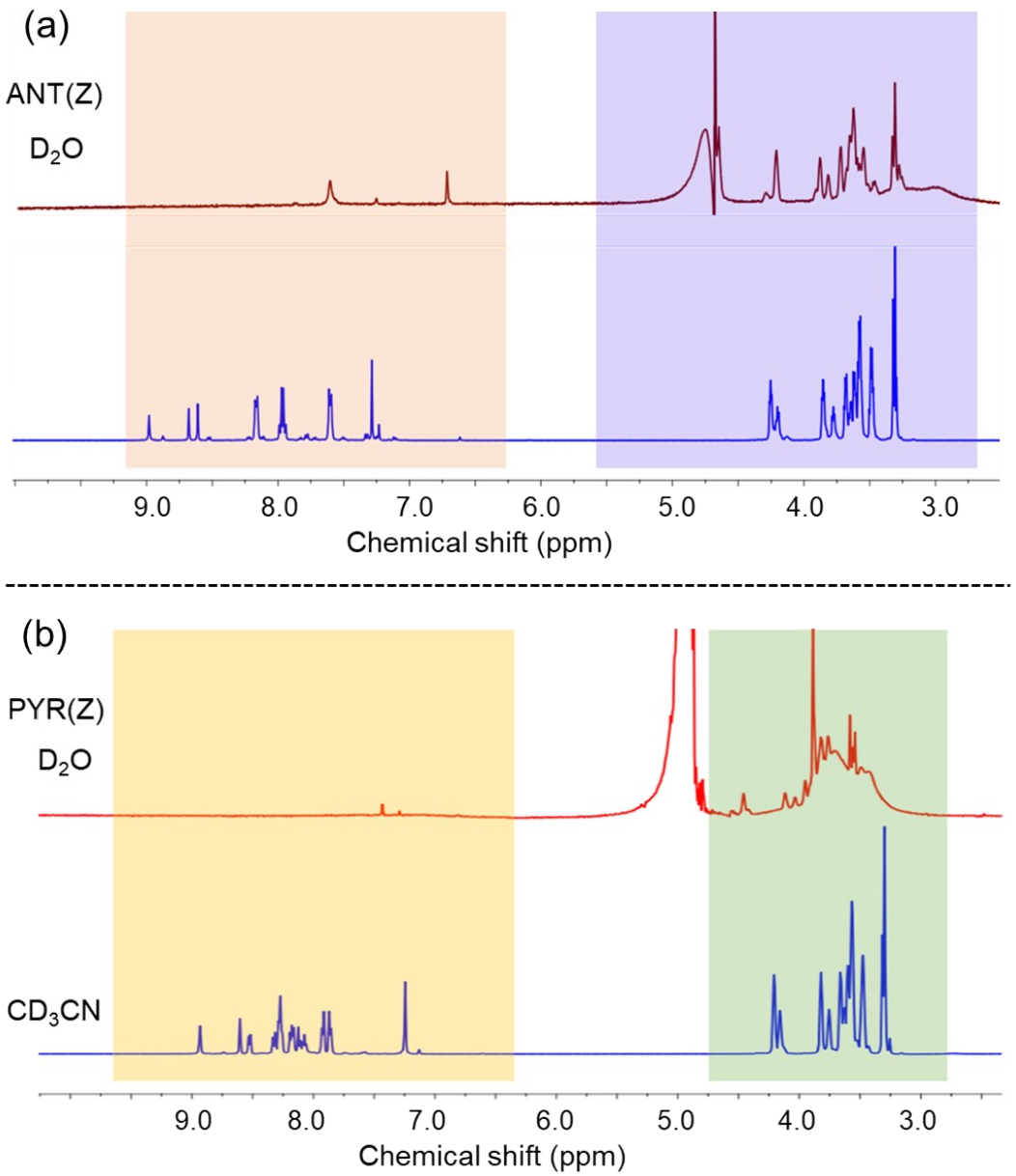

Figure S4. (a) ^{1}H NMR spectra of **ANT(Z)** in CD_3CN and D_2O medium, indicative of molecular assembly in water through non-covalent interactions. (b) ^{1}H NMR spectra of **PYR(Z)** in CD_3CN and D_2O medium, indicative of molecular assembly in water through non-covalent interactions.

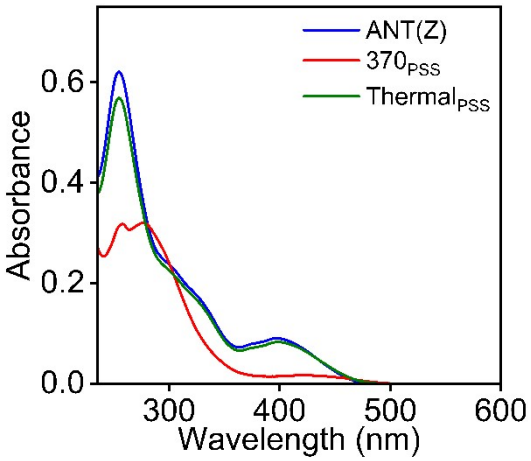

Figure S5. Absorption spectra of **ANT(Z)** in water before and after irradiation at 370 nm (370_{PSS}) and thermal condition ($Thermal_{PSS}$). Calculated isomer ratios were 14:86 (*Z*:*E*) at 370_{PSS} and 90:10 (*Z*:*E*) at $Thermal_{PSS}$.

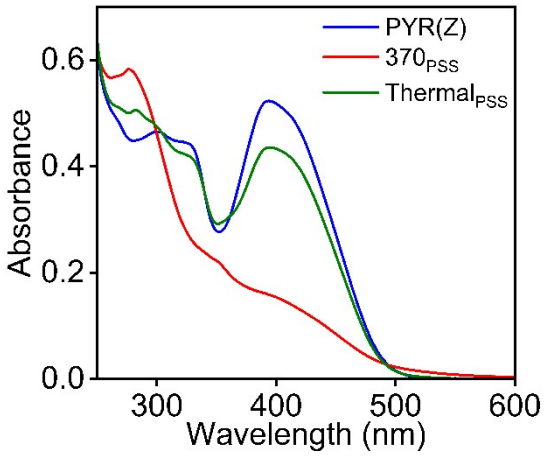

Figure S6. Absorption spectra of **PYR(Z)** in water before and after irradiations at 370 nm (370_{PSS}) and thermal condition ($Thermal_{PSS}$). Calculated isomer ratios were 30:70 (*Z*:*E*) at 370_{PSS} and 84:16 (*Z*:*E*) at $Thermal_{PSS}$.

(a) (b)

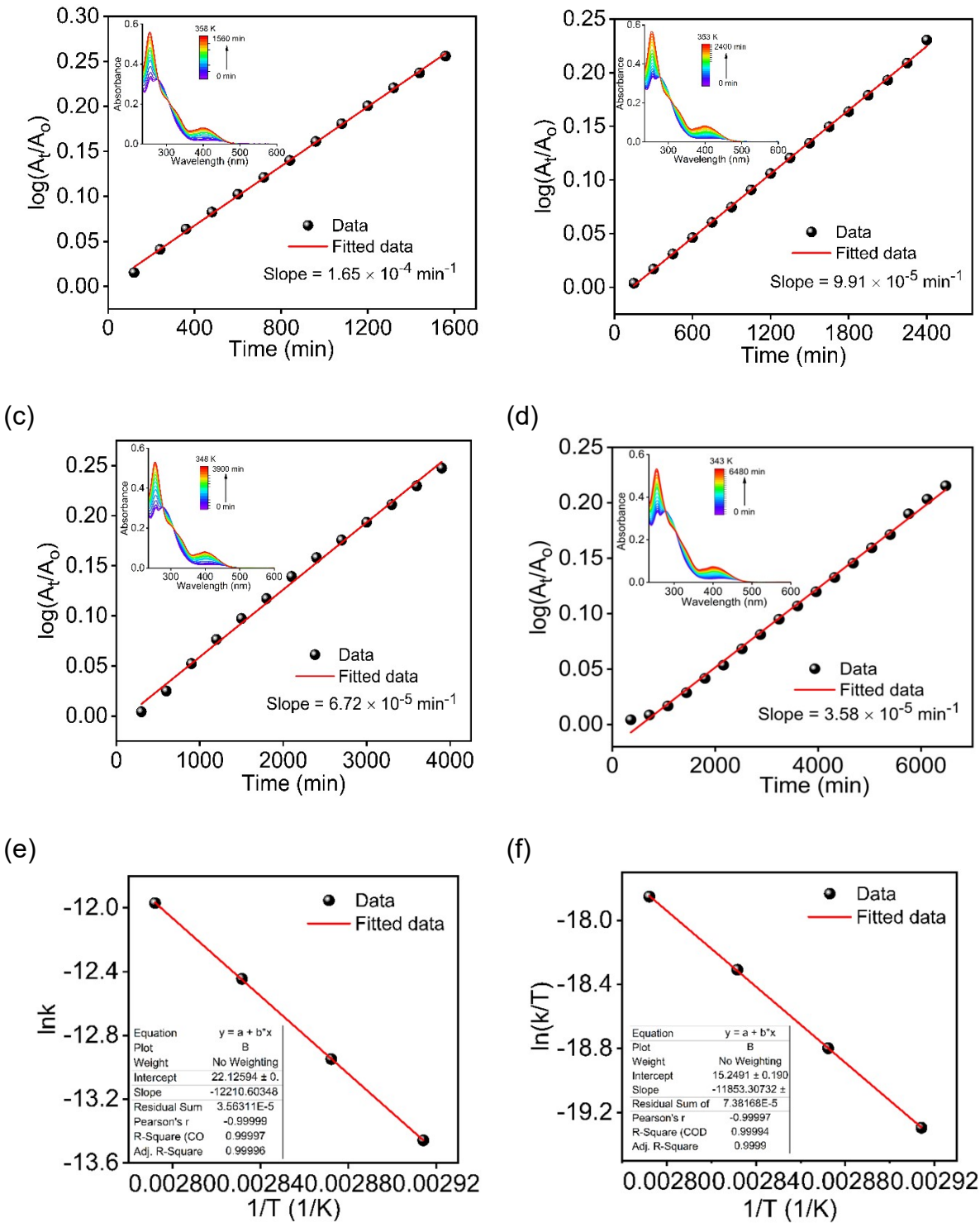

Figure S7. Thermal back isomerization of **ANT(E)** to **ANT(Z)** at different temperatures (a) 358, (b) 353, (c) 348, (d) 343 K in aqueous medium as a function of time, assuming first-order kinetics for the thermal reversal. The corresponding UV-Vis spectral changes are shown in the inset. (e) Arrhenius plot and (f) Eyring plot of thermal back isomerization of **ANT(E)** to **ANT(Z)** in aqueous medium. we got slope = $-(\Delta H^{\neq}/R)$ and intercept = $\ln(k_B/h) + \Delta S^{\neq}/R$.

(a) (b)

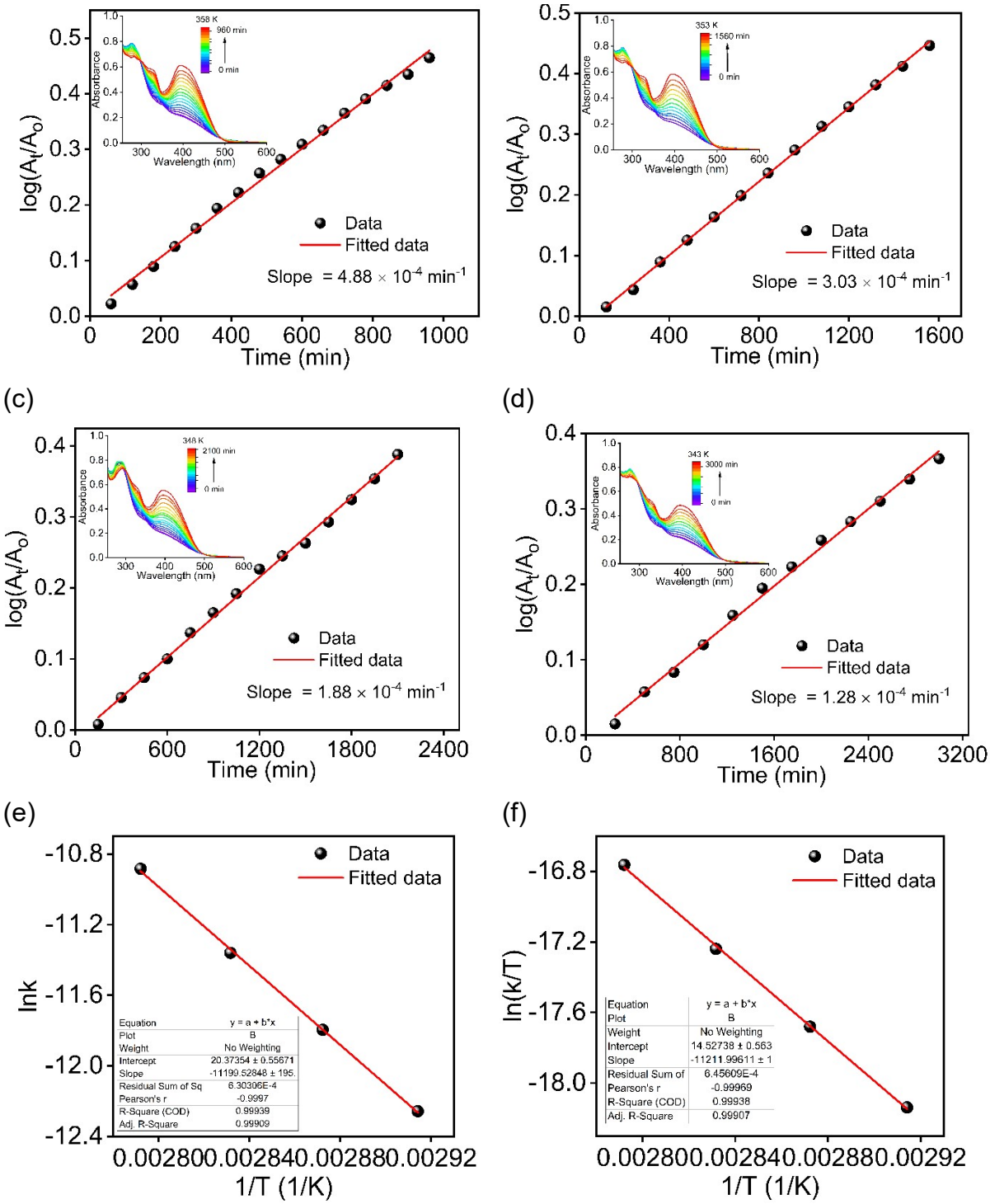

Figure S8. Thermal back isomerization of **PYR(E)** to **PYR(Z)** at different temperatures (a) 358, (b) 353, (c) 348, (d) 343 K in aqueous medium as a function of time, assuming first-order kinetics for thermal reversal. The corresponding UV-Vis spectral changes are shown in the inset. (e) Arrhenius plot and (f) Eyring plot of thermal back isomerization of **PYR(E)** to **PYR(Z)** in aqueous medium. we got slope = $-(\Delta H^{\neq}/R)$ and intercept = $\ln(k_B/h) + \Delta S^{\neq}/R$.

Table S1. Thermodynamic parameters of thermal back isomerization of **ANT(E)** in water.

Sample	E_a ($kJmol^{-1}$)	$\Delta H^{\#}$ ($kJmol^{-1}$)	$\Delta S^{\#}$ ($Jmol^{-1}K^{-1}$)	$t_{1/2}$ at 298 K
ANT(E)	102	98.55	-70.76	0.64 ± 0.02 years

Table S2. Thermodynamic parameters of thermal back isomerization of **PYR(E)** in water.

Sample	E_a ($kJmol^{-1}$)	$\Delta H^{\#}$ ($kJmol^{-1}$)	$\Delta S^{\#}$ ($Jmol^{-1}K^{-1}$)	$t_{1/2}$ at 298 K
PYR(E)	93.1	93.21	-76.76	3.3 ± 0.17 years

(a) (b)

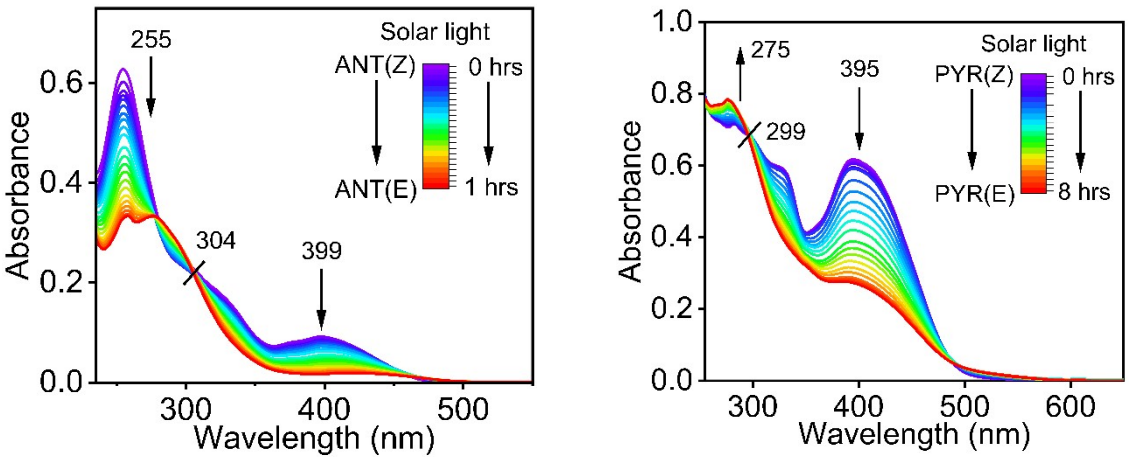

Figure S9. Time-dependent UV-vis absorption spectral change of (a) **ANT** and (b) **PYR** (5×10^{-5} M) in aqueous medium under solar light using a Newport Class A solar simulator.

(a) (b)

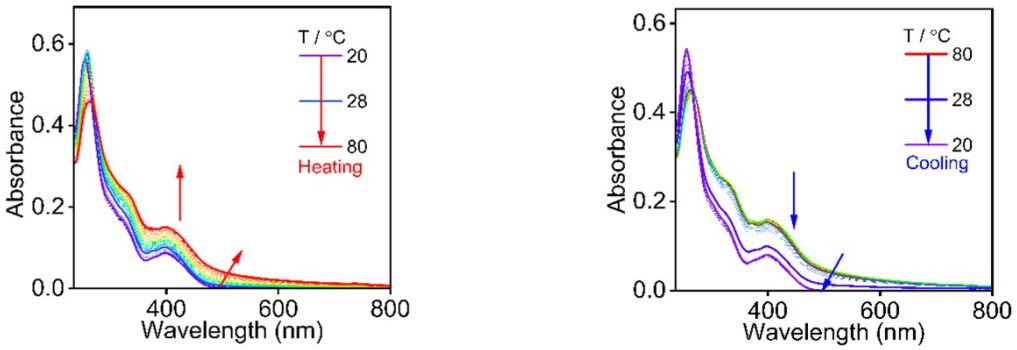

Figure S10. Variable-temperature (a) heating and (b) cooling curve of **ANT(Z)** (5×10^{-5} M) in water.

(a) (b)

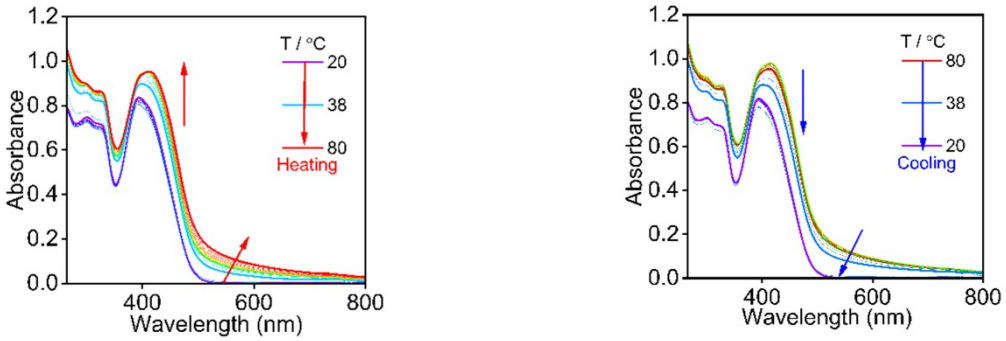

Figure S11. Variable-temperature (a) heating and (b) cooling curve of **PYR(Z)** (5×10^{-5} M) in water.

(a)

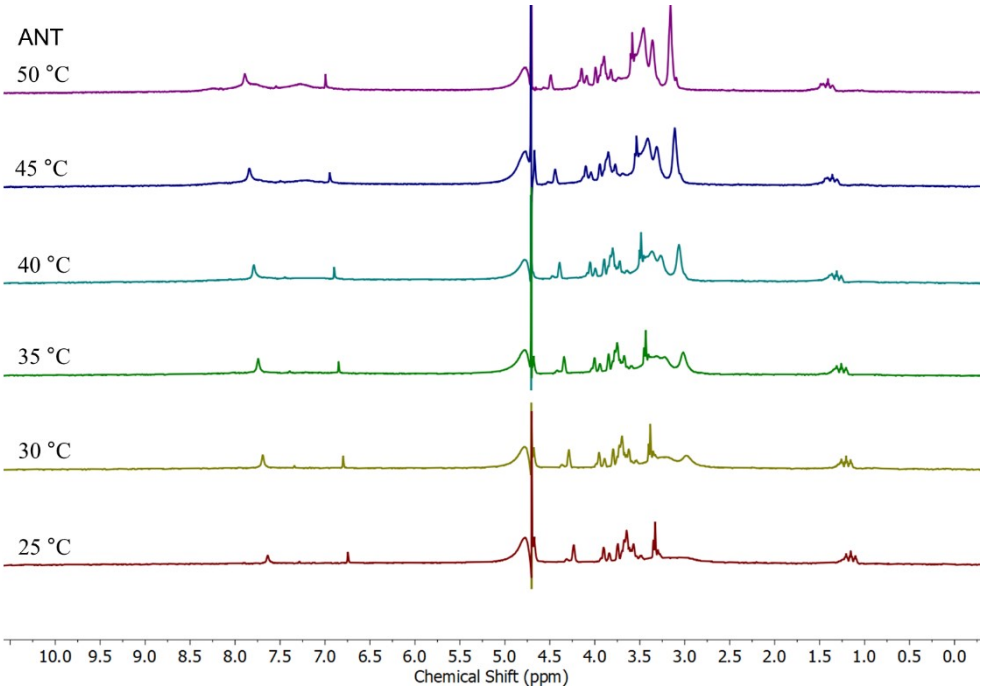

(b)

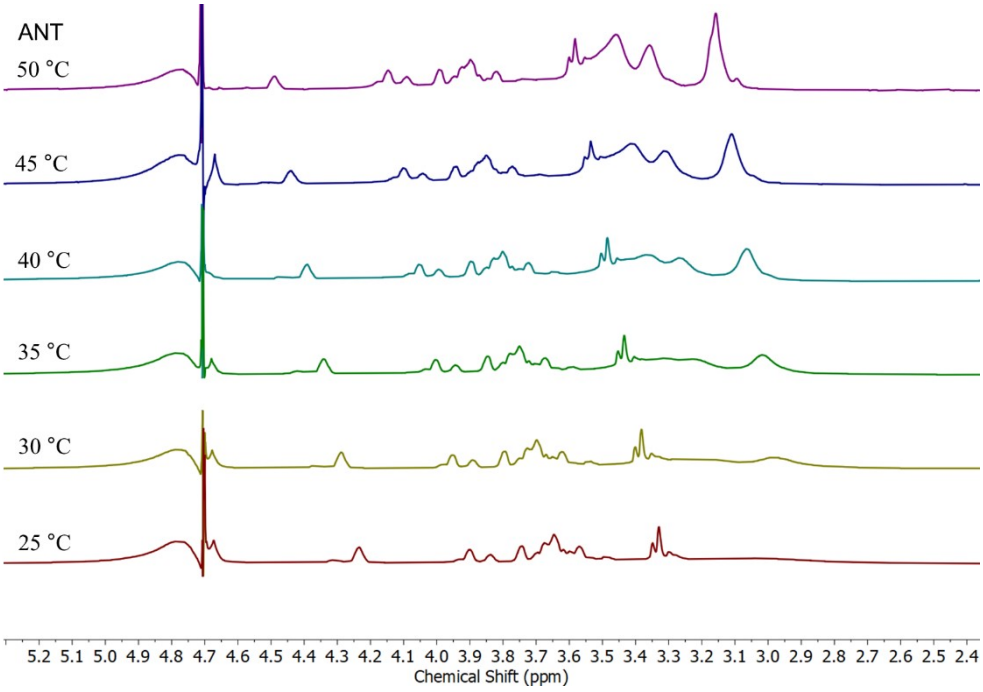

Figure S12. (a) Variable-temperature ^{1}H NMR spectra of **ANT(Z)** (10 mM, D_2O, 500 MHz). (b) Variable-temperature partial ^{1}H NMR spectra exhibited download ^{1}H NMR shift because of disruption of intermolecular-hydrogen bonding between water and oligoethylene glycol unit in aqueous medium.

(a)

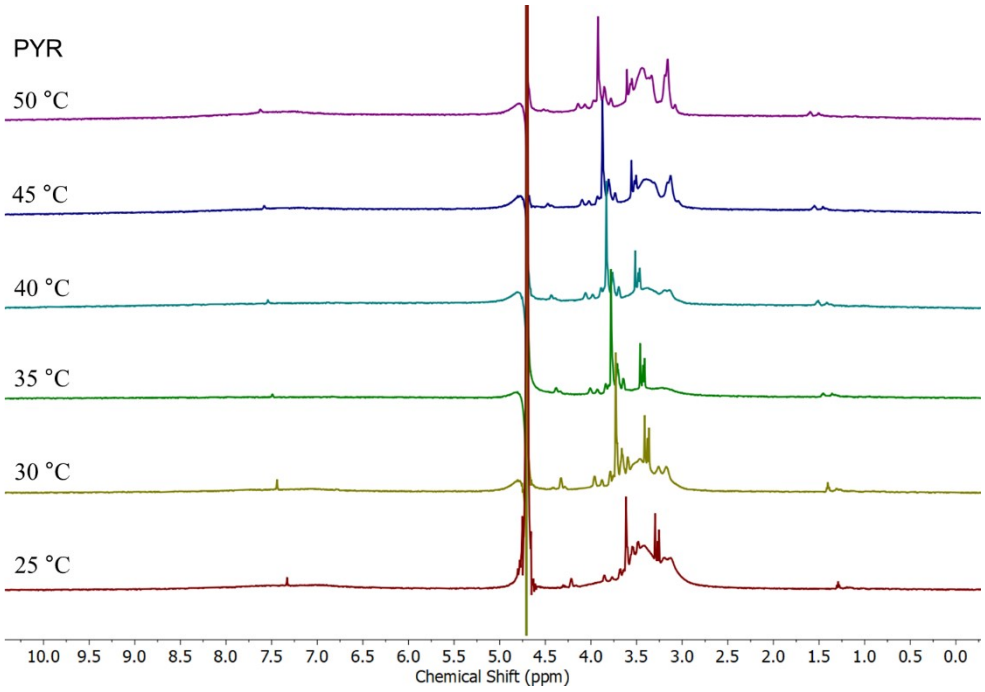

(b)

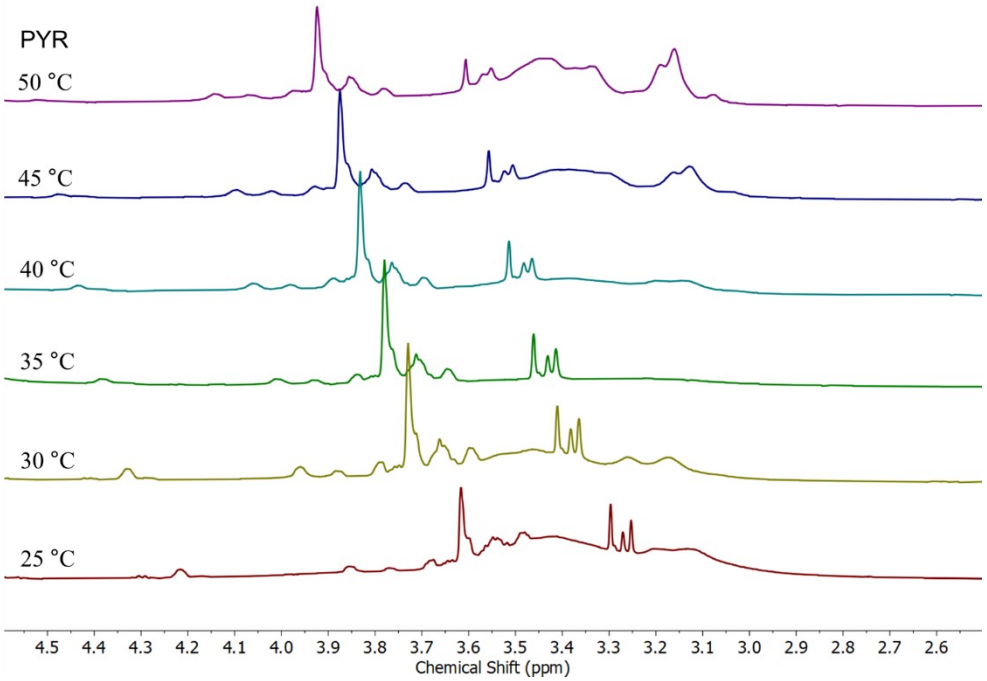

Figure S13. (a) Variable-temperature ^{1}H NMR spectra of **PYR(Z)** (10 mM, D_2O, 500 MHz). (b) Variable-temperature partial ^{1}H NMR spectra exhibited download ^{1}H NMR shift because of disruption of intermolecular-hydrogen bonding between water and oligoethylene glycol unit in aqueous medium.

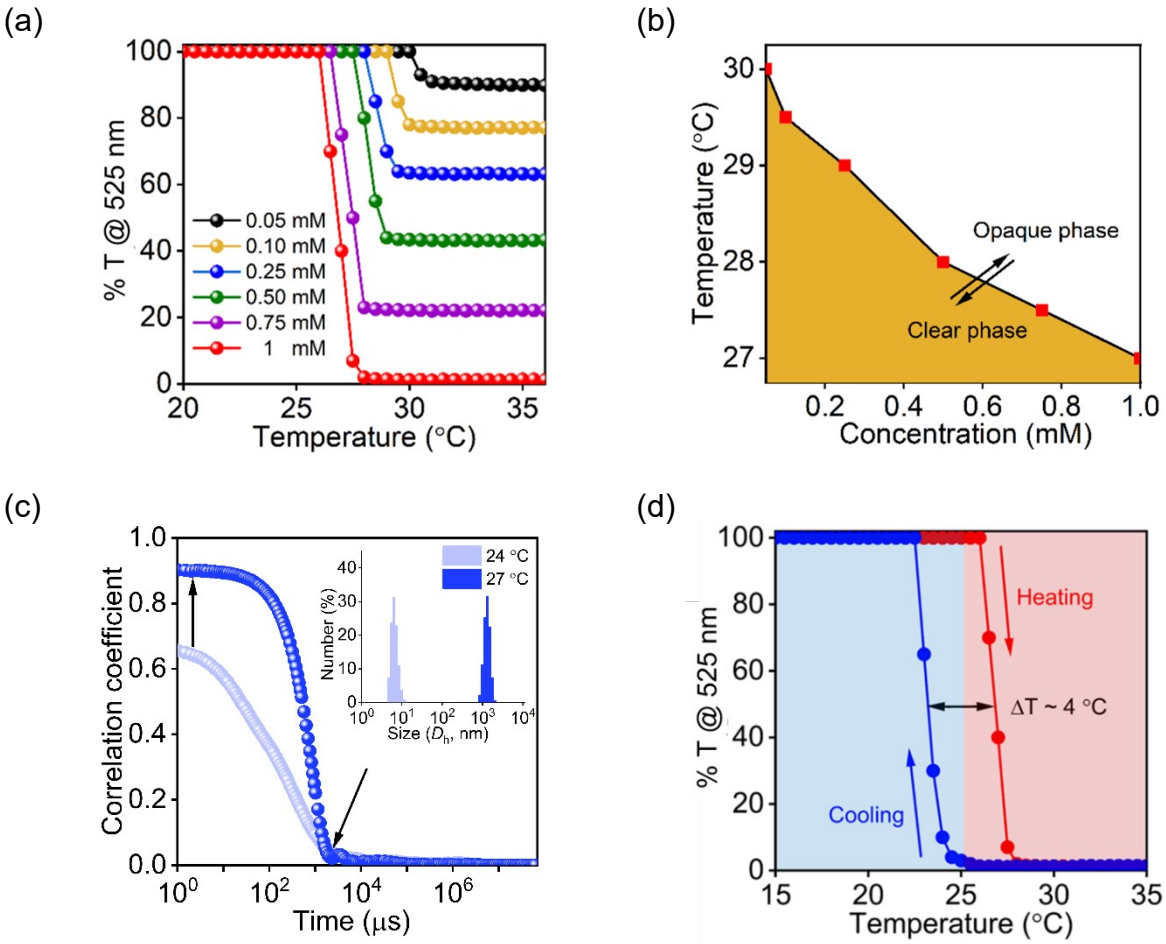

Figure S14. (a) Transmittance spectra of the phase change of **ANT(Z)** as a function of temperature at various concentrations in aqueous medium. (b) Phase diagram with the increasing concentration of **ANT(Z)**. (c) DLS correlation decay plot showing a sigmoidal curve at 300 K fitted with a mono-exponential decay model, suggesting the formation of spherical nanoparticles in an aqueous medium. Inset shows the plot of number of particles vs size below and above LCST. Particle size increases with the increase in temperature. (d) Thermal hysteresis for heating and cooling cycle (heating and cooling rate 2 °C/ min).

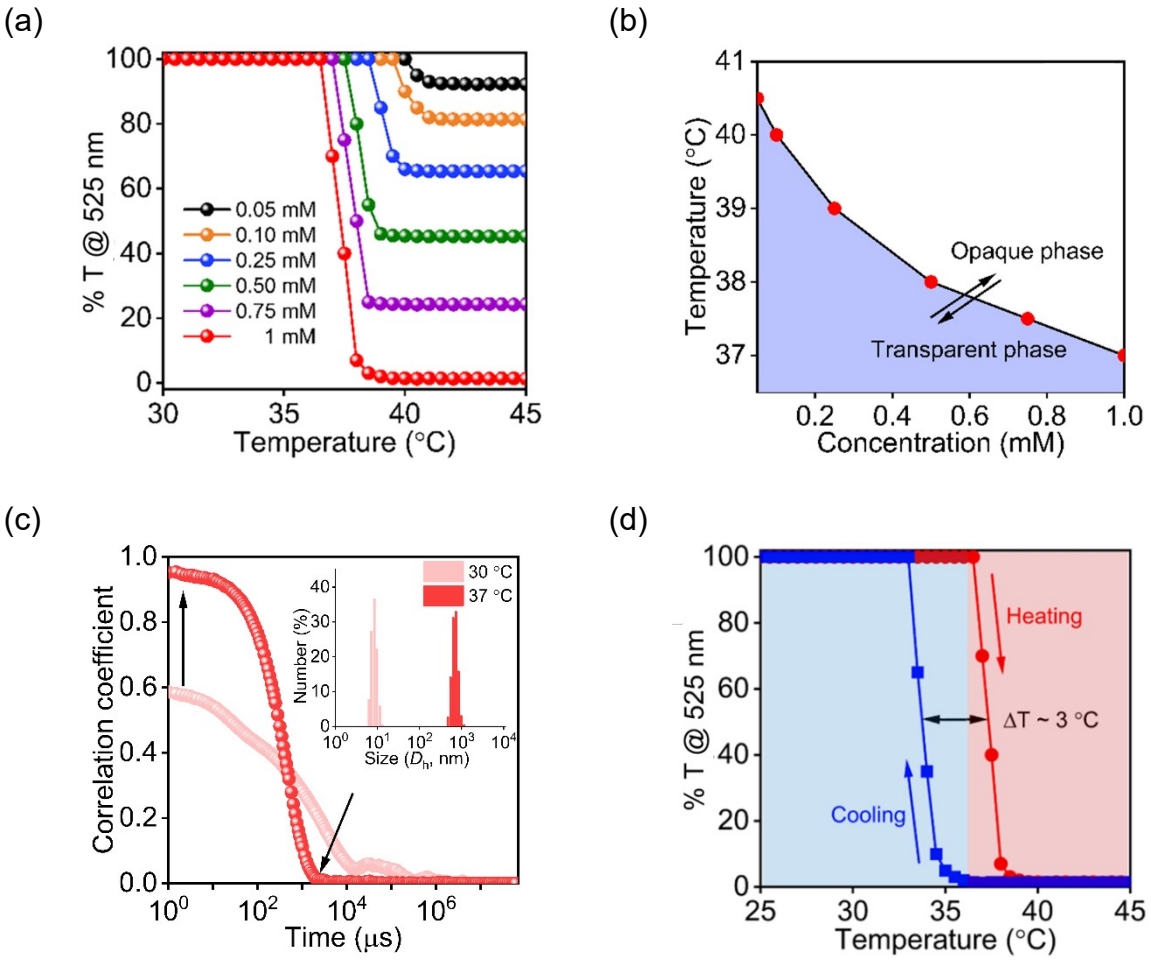

Figure S15. (a) Transmittance spectra of the phase change of **PYR(Z)** as a function of temperature and at various concentrations in aqueous medium. (b) Phase diagram with the increasing concentration of **PYR(Z)**. (c) DLS correlation decay plot showing a sigmoidal curve at 300 K fitted with a mono-exponential decay model, suggesting the formation of spherical nanoparticles in an aqueous medium. Inset shows the plot of number of particles vs size below and above LCST. Particle size increases with the increase in temperature. (d) Thermal hysteresis for heating and cooling cycle (heating and cooling rate 2 °C/ min).

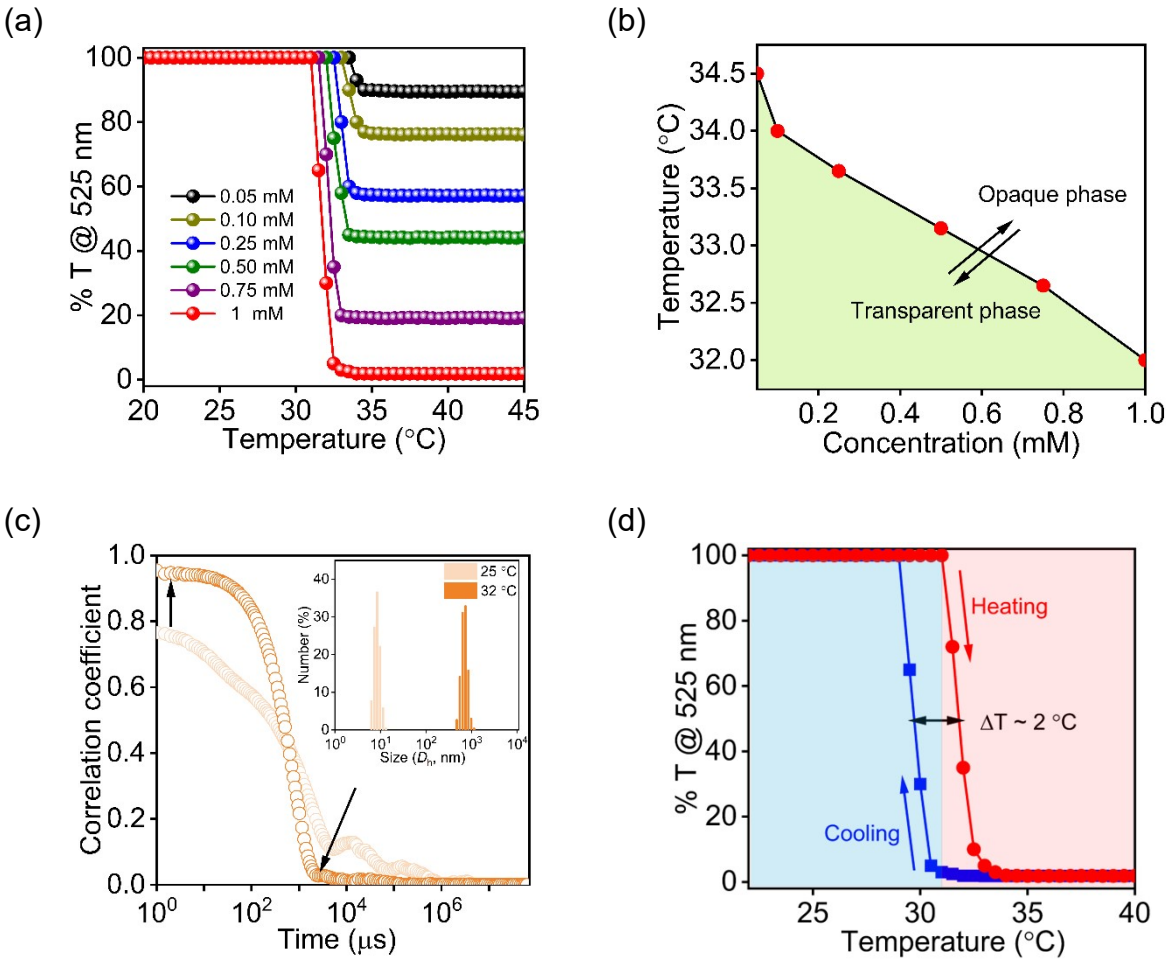

Figure S16. (a) Transmittance spectra of the phase change of **ANT(Z)/PYR(Z)** (1:1) as a function of temperature and at various concentrations in aqueous medium. (b) Phase diagram with the increasing concentration of **ANT(Z)/PYR(Z) (1:1)**. (c) DLS correlation decay plot showing a sigmoidal curve at 300 K fitted with a mono-exponential decay model, suggesting the formation of spherical nanoparticles in an aqueous medium. Inset shows the plot of number of particles vs size below and above LCST. Particle size increases with the increase in temperature. (d) Thermal hysteresis for heating and cooling cycle (heating and cooling rate 2 °C/ min).

(a) (b)

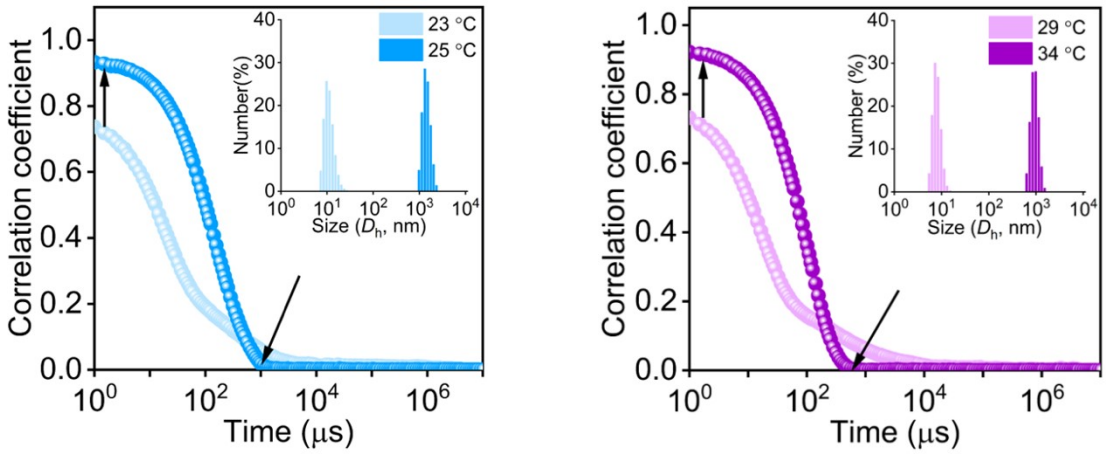

Figure S17. Variable-temperature dynamic light scattering behavior of (a) **ANT** and (b) **PYR** after photoirradiation.

(a) (b)

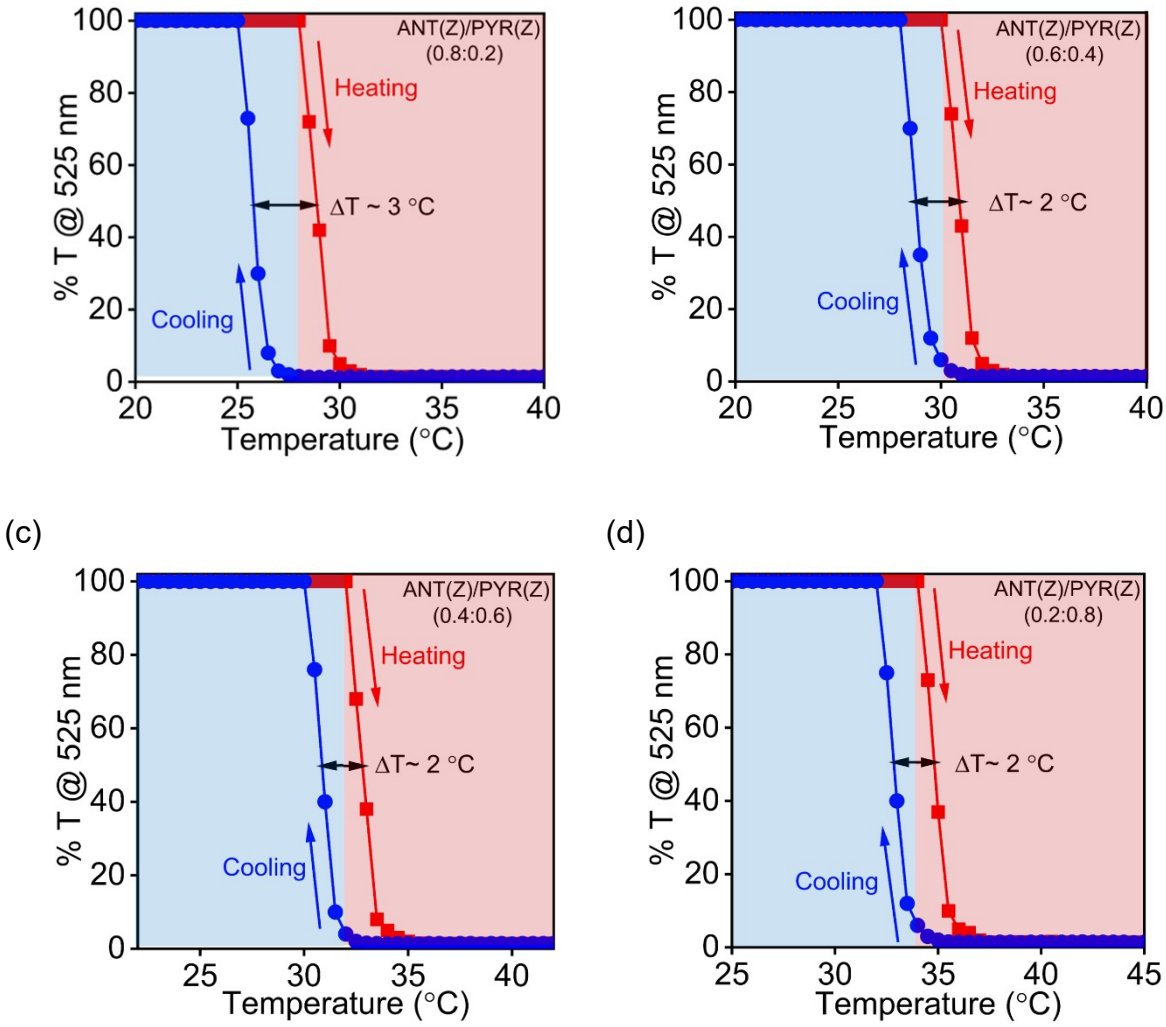

Figure S18. Thermal hysteresis of the co-assembled state of **ANT(Z)/PYR(Z)** at different ratios for heating and cooling cycle (heating and cooling rate 2 °C/ min).

Density functional theory calculations

The density functional theory (DFT) calculations were performed using the Density Functional Theory (DFT) method, specifically employing Becke's three-parameter hybrid exchange functional combined with the Lee-Yang-Parr correlation functional, abbreviated as B3LYP. The 6-31+g (d,p) basis set was utilized alongside a Polarizable Continuum Model (PCM) for water, as implemented in Gaussian 09 (G09). To reduce the computational complexity, the long triethylene glycol monomethyl ether chain was truncated to only the corresponding methoxy fragments. All geometries of **ANT(Z)**, **ANT(E)**, **PYR(Z)**, and **PYR(E)** were optimized without any imaginary frequencies using the Gaussian software package. The visualization of molecular orbitals was conducted using the 'Gauss View' software.

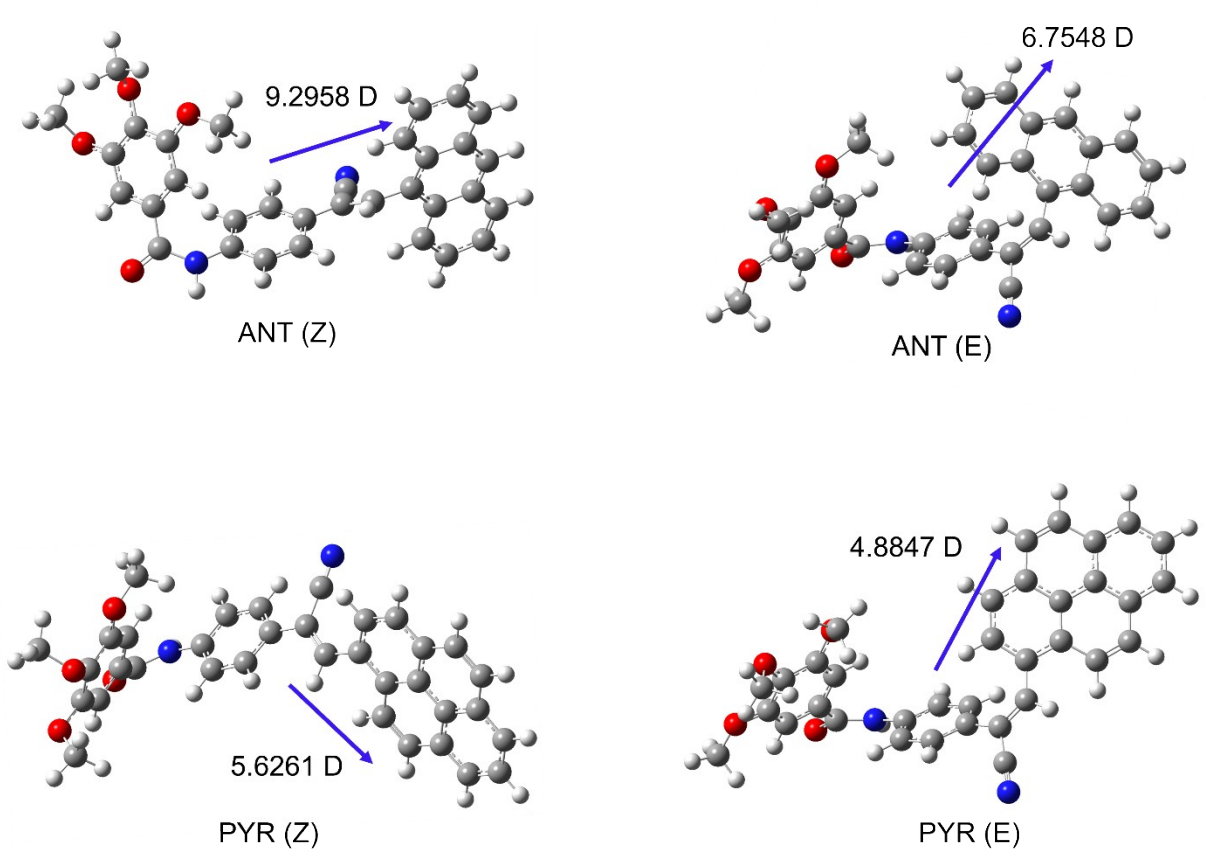

Figure S19. Calculated dipole moment of **ANT(Z)**, **ANT(E)**, **PYR(Z)**, and **PYR(E)** at B3LYP/6-31G (d, p) level of DFT.

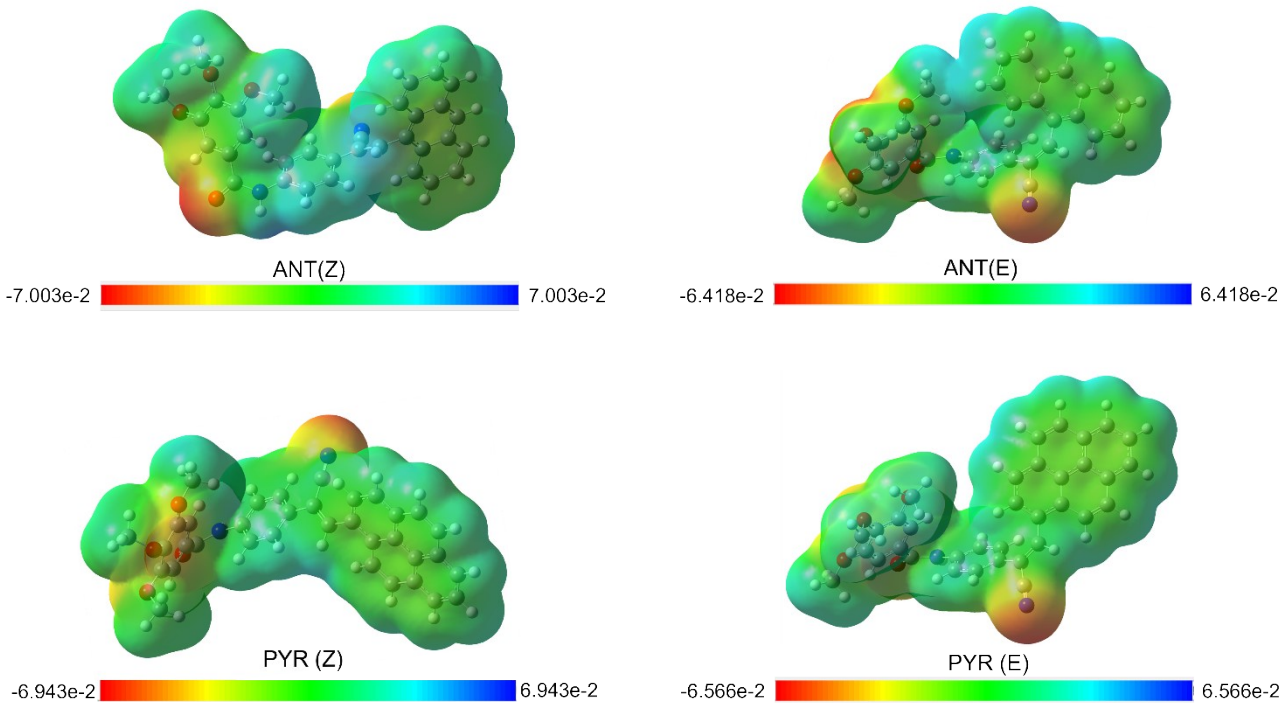

Figure S20. The molecular electrostatic potential surface of **ANT(Z)**, **ANT(E)**, **PYR(Z)**, and **PYR(E)** at B3LYP/6-31G (d, p) level of DFT.

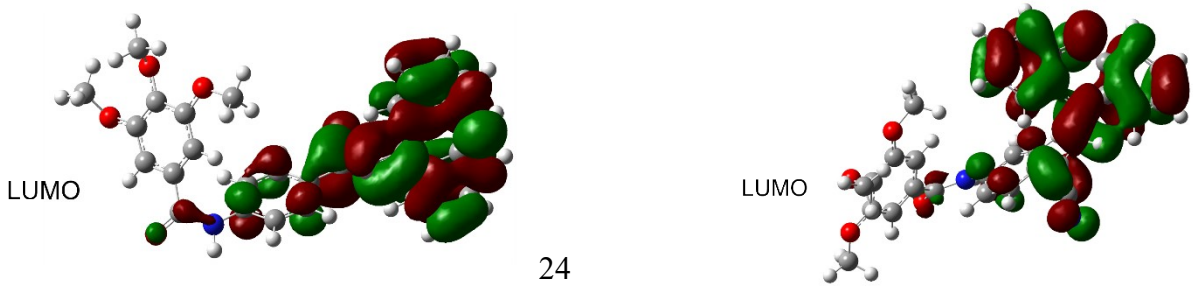

Figure S21. The frontier orbitals, HOMO, and LUMO of **ANT(Z)** and **ANT(E)** at B3LYP/6-31G (d, p) level of DFT.

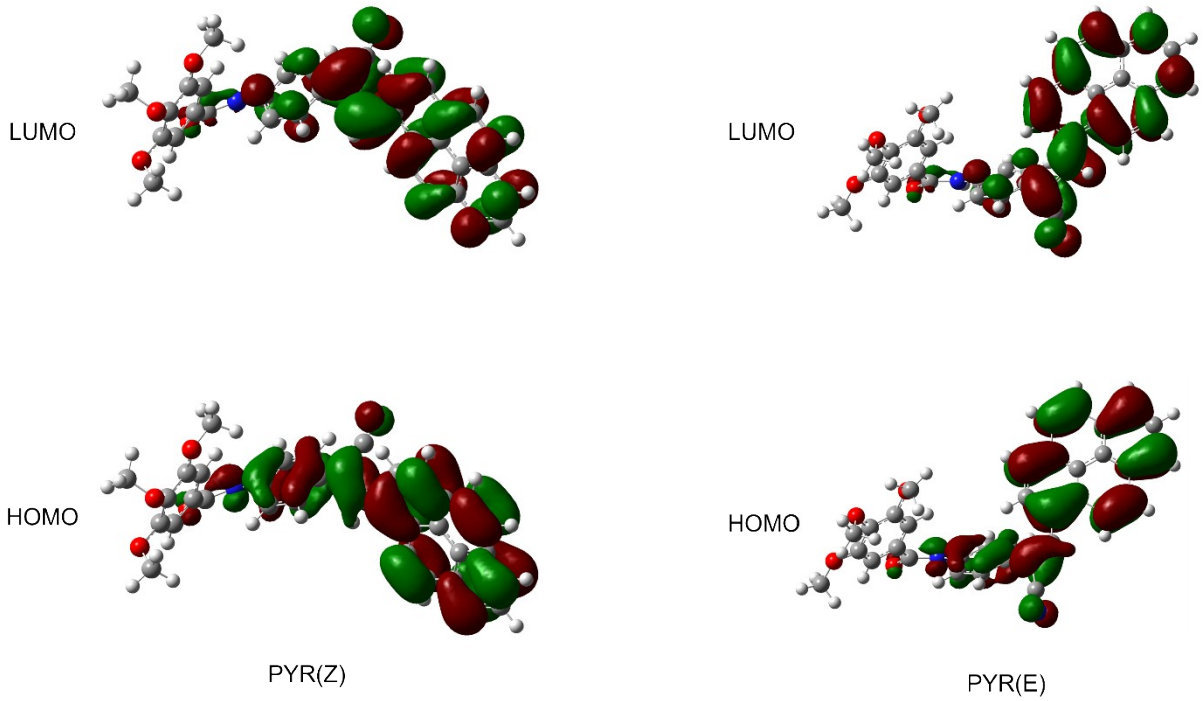

Figure S22. The frontier orbitals, HOMO, and LUMO of **PYR(Z)** and **PYR(E)** at B3LYP/6-31G(d, p) level of DFT.

Table S3. Cartesian coordinates of the optimized geometries of **ANT(Z)**, **ANT(E)**, **PYR(Z)**, and **PYR(E)**. Atomic number followed by X, Y, Z coordinates in Å.
Level of theory: B3LYP/6-31G(d,p) cpcm model, solvent = water

Atomic numbers and their X, Y, Z Coordinates of ANT(Z)

C	4.34121300	-0.13117300	-0.22544700
C	2.99123700	0.32230600	-0.60618400
C	2.05297900	0.90468500	0.18604100
C	0.73156600	1.37251400	-0.30266200
C	-0.37674100	1.43816400	0.55900800
C	-1.62391000	1.85281300	0.10488200
C	-1.80306800	2.19605000	-1.24282500
C	-0.69811800	2.15761000	-2.10654000
C	0.55028800	1.76444600	-1.64020800
N	-3.03786700	2.65223400	-1.75727500
C	-4.33855200	2.40104200	-1.36950000
C	-4.65700400	1.14306700	-0.62238000
O	-5.22863100	3.18625000	-1.69881300
H	-2.98341900	3.41575700	-2.42219500
C	-5.68307300	1.18986900	0.31868200
C	-6.08346600	0.03039200	0.99235600
C	-5.45958300	-1.19762800	0.70836500
C	-4.42578500	-1.23799400	-0.26036100
C	-4.03284100	-0.07675200	-0.92597100
O	-7.03884900	0.19581900	1.95715400
O	-5.78643200	-2.30934300	1.44243300
O	-3.85207600	-2.45914000	-0.44987500
C	-8.12772200	-0.73552900	2.03778800
C	-6.37851800	-3.41042600	0.72637800
C	-2.76716500	-2.56276200	-1.37258700
C	5.31019500	0.75982400	0.31023500
C	6.62131100	0.25353600	0.65413900
C	6.92718800	-1.09140300	0.42670100
C	5.99796100	-1.97133100	-0.13846500
C	4.67888600	-1.48993600	-0.47102400
C	6.32614000	-3.34155100	-0.38289200
C	5.40782300	-4.20074900	-0.92592400
C	4.10072400	-3.73476000	-1.24283900
C	3.74553200	-2.42901300	-1.01406800
C	5.07993200	2.16291900	0.48390300

C	6.04514400	2.98647000	1.00359900
C	7.31742800	2.47268600	1.38518200
C	7.59578900	1.14479100	1.20615300
H	2.69549100	0.12612600	-1.63466400
C	2.29615200	1.03618000	1.59729100
N	2.44454600	1.13836500	2.74748600
H	-0.26347100	1.17081500	1.60479600
H	-2.45384900	1.91566700	0.79816400
H	-0.82041200	2.44835400	-3.14542400
H	1.39262700	1.77748400	-2.32349400
H	-6.18911200	2.12249700	0.53755000
H	-3.25034600	-0.11250900	-1.67122700
H	-8.91479700	-0.22259300	2.59386900
H	-8.50168300	-0.98873800	1.03987200
H	-7.83875000	-1.64728900	2.56275600
H	-6.60593400	-4.16664600	1.47904400
H	-7.30574600	-3.09723400	0.23439100
H	-5.68715600	-3.81810300	-0.01275000
H	-2.45313200	-3.60599700	-1.34413900
H	-3.08146800	-2.30520000	-2.38996900
H	-1.93072500	-1.92097400	-1.07516400
H	7.91603200	-1.46045000	0.68709500
H	7.32395000	-3.68575900	-0.12550200
H	5.66752500	-5.23873000	-1.10906800
H	3.37478100	-4.42501700	-1.66170800
H	2.73461600	-2.10637900	-1.23754800
H	4.12897900	2.58388200	0.18140600
H	5.84150300	4.04680600	1.11840400
H	8.06503500	3.14068900	1.80141700
H	8.56897000	0.74053600	1.47046200

Atomic numbers and their X, Y, Z Coordinates of ANT(E)

H	-4.09088500	0.84878800	2.71833400
C	-3.43007000	0.72353800	1.86185400
C	-2.23399400	1.36474100	1.93200500
C	-1.19008100	1.48998400	0.88198200
C	0.16288100	1.62588100	1.23651000
C	1.15359600	1.79653800	0.27538200
C	0.81366700	1.82214200	-1.08501100
C	-0.53648700	1.69823500	-1.44944800
C	-1.52151700	1.54319900	-0.48249800
N	1.75602400	2.04972800	-2.11191700
C	3.12641300	1.88134900	-2.15561400
C	3.77226500	0.85343800	-1.28019600
O	3.78880000	2.53390600	-2.96287800
H	1.42542500	2.61510900	-2.88615400
C	5.03917000	1.15005400	-0.76651800
C	5.71386900	0.19469700	0.00091800
C	5.13531100	-1.07153600	0.21022800
C	3.87103700	-1.36662900	-0.33466200

C	3.18231600	-0.39928000	-1.07480500
O	6.93157700	0.38444600	0.57744800
O	5.83481700	-2.03044700	0.89899800
O	3.41182900	-2.62435900	-0.08875400
C	7.56875600	1.64899000	0.39702800
C	5.45562700	-2.16816600	2.27763200
C	2.13720800	-2.99035800	-0.61686700
C	-3.96567700	-0.11826000	0.76966000
C	-3.34390800	-1.34169400	0.40952000
C	-3.94068900	-2.15978200	-0.62320300
C	-5.12630500	-1.74492400	-1.23827200
C	-5.76604200	-0.55623900	-0.87192200
C	-5.18069900	0.27582900	0.15257200
C	-6.98681900	-0.14391500	-1.49266900
C	-7.60389500	1.02369400	-1.12904400
C	-7.02512900	1.85261200	-0.12603900
C	-5.85110500	1.49566200	0.48743500
C	-2.16383200	-1.83807400	1.05050900
C	-1.60431700	-3.03519300	0.68348400
C	-2.17825500	-3.82277800	-0.35567700
C	-3.31527800	-3.39485400	-0.98618800
C	-1.95555200	2.04462400	3.17148600
N	-1.71782000	2.59701900	4.16857700
H	0.44862700	1.61922000	2.28380600
H	2.18266300	1.92851200	0.58547200
H	-0.81269200	1.73756700	-2.49882400
H	-2.55750700	1.47736000	-0.79232900
H	5.47255300	2.12015500	-0.96910700
H	2.21297200	-0.61682500	-1.50225900
H	8.51072500	1.58693900	0.94210500
H	7.77395200	1.84630100	-0.66104500
H	6.96350300	2.46466300	0.80816300
H	6.09011000	-2.95270600	2.69384000
H	5.62601700	-1.23418800	2.82438800
H	4.40518000	-2.46205700	2.36830300
H	1.97156400	-4.02128100	-0.30378600
H	1.33905400	-2.35620100	-0.21584200
H	2.12881400	-2.93779500	-1.71130500
H	-5.56676800	-2.36739100	-2.01304500
H	-7.41402800	-0.78080400	-2.26223600
H	-8.53105300	1.32603300	-1.60593500
H	-7.51713300	2.78066400	0.14875600
H	-5.41511400	2.15235400	1.23284600
H	-1.71757400	-1.26114200	1.85128500
H	-0.71751700	-3.39411400	1.19682800
H	-1.71605200	-4.76464300	-0.63440300
H	-3.77323600	-3.99126500	-1.77038800

Atomic numbers and their X, Y, Z Coordinates of PYR(Z)

C	3.32060900	0.66640700	0.55407800
C	2.00528200	0.87694200	-0.04229800

C	1.12681300	1.90270500	0.15233400
C	-0.23244500	1.93198200	-0.44523700
C	-0.86951200	3.15146000	-0.73357700
C	-2.13301600	3.18238900	-1.31182500
C	-2.80075700	1.99079400	-1.62698900
C	-2.17252500	0.76692300	-1.35318200
C	-0.91866500	0.74364800	-0.75319800
N	-4.06334000	2.07630700	-2.25919000
C	-5.14326700	1.21844500	-2.25790700
C	-5.32716500	0.26370800	-1.11819300
O	-5.97657400	1.29091500	-3.16208400
H	-4.15512800	2.79984900	-2.96371700
C	-5.89548600	-0.98003500	-1.39921100
C	-6.16397500	-1.87324000	-0.36025100
C	-5.88143600	-1.52005100	0.96682500
C	-5.31921700	-0.25453700	1.24871800
C	-5.03994200	0.63156700	0.20554900
O	-6.77051200	-3.07085600	-0.65475800
O	-6.12099600	-2.41262000	1.98157200
O	-5.09828800	0.00374400	2.56632500
C	-5.94944100	-4.23699900	-0.47836100
C	-7.34872700	-2.18627000	2.69567000
C	-4.52629800	1.26399000	2.91911800
H	1.67509800	0.11485900	-0.74131400
C	4.34025700	-0.01121300	-0.18019000
C	5.60183700	-0.26451800	0.44623100
C	5.83820500	0.15840700	1.79095800
C	4.81071500	0.82166000	2.48313400
C	3.58767600	1.06441000	1.87914500
C	4.17166600	-0.43147700	-1.54503400
C	5.16024600	-1.08137600	-2.22283300
C	6.42669800	-1.36457000	-1.61335500
C	6.63891800	-0.94157500	-0.26709200
C	7.89640100	-1.19878300	0.36245100
C	8.09471500	-0.76190000	1.71648000
C	7.11006700	-0.11250900	2.39837400
C	7.45799100	-2.03147500	-2.29719100
C	8.67883900	-2.28093000	-1.67331500
C	8.89820500	-1.86955000	-0.35892200
C	1.49954800	3.06430400	0.90865700
N	1.75640500	4.04224200	1.48781600
H	-0.37265600	4.08865700	-0.50441700
H	-2.61029500	4.13480700	-1.52086100
H	-2.66476300	-0.16565400	-1.60171400
H	-0.47363000	-0.21737000	-0.51819600
H	-6.14148400	-1.25760800	-2.41735900
H	-4.61974200	1.60616700	0.41373700
H	-6.56475900	-5.08891600	-0.77240800
H	-5.06502500	-4.18820200	-1.12422600
H	-5.64055400	-4.34752100	0.56411400
H	-7.40764900	-2.96553400	3.45711300

H	-7.34492700	-1.20355900	3.17657800
H	-8.20867400	-2.26682600	2.02225600
H	-4.42773600	1.25150200	4.00446100
H	-3.53781700	1.39315800	2.46477200
H	-5.17595900	2.09485600	2.62226500
H	4.97586900	1.12921300	3.51150300
H	2.80385300	1.53918200	2.45733200
H	3.24277500	-0.21348700	-2.05891300
H	5.00102300	-1.38870400	-3.25261700
H	9.05259900	-0.96026400	2.18902100
H	7.27157600	0.21409500	3.42168900
H	7.29248700	-2.35090200	-3.32217700
H	9.46546700	-2.79770300	-2.21438300
H	9.85265800	-2.06580900	0.12127300

Atomic numbers and their X, Y, Z Coordinates of PYR(E)

H	-3.01031400	2.40087200	2.27528300
C	-2.34994500	1.94693500	1.54075300
C	-1.14060500	2.55533700	1.38207500
C	-0.09332000	2.27159700	0.36334800
C	1.26771400	2.30610300	0.70761400
C	2.25951000	2.08242300	-0.24211000
C	1.90820800	1.80199300	-1.56993300
C	0.55180800	1.79056500	-1.92929900
C	-0.43258100	2.03021100	-0.97819600
N	2.87143700	1.60226000	-2.58596500
C	4.15679100	1.10378500	-2.53578500
C	4.54535000	0.17447900	-1.42811200
O	4.94890700	1.37904200	-3.43836000
H	2.67184800	2.04507500	-3.47597700
C	3.66993100	-0.78590000	-0.92440000
C	4.10344200	-1.69655600	0.04723800
C	5.42566700	-1.64519800	0.52231500
C	6.31245400	-0.67528200	-0.00906000
C	5.87348800	0.22350900	-0.97971300
O	3.19703900	-2.65127800	0.42106400
O	5.86685300	-2.59932100	1.40371700
O	7.58822000	-0.72913300	0.46550200
C	3.02923100	-2.95312600	1.81404500
C	6.27516200	-2.13673200	2.70561000
C	8.54035400	0.20343300	-0.04732600
C	-2.86032100	0.73301200	0.89995100
C	-4.25010800	0.59850000	0.62011900
C	-4.74123200	-0.63938000	0.09559300
C	-3.84578500	-1.72670400	-0.14332300
C	-2.48023200	-1.55640200	0.14580900
C	-2.00434900	-0.35767500	0.65168000
C	-5.19098200	1.66860700	0.81596300
C	-6.51781100	1.51383800	0.54416300
C	-7.04016500	0.27872100	0.03473100

C	-6.13173100	-0.79865200	-0.19207200
C	-6.62182800	-2.03802100	-0.70902000
C	-5.69197300	-3.10962400	-0.93381000
C	-4.36483900	-2.95961700	-0.66358200
C	-8.40436700	0.10078400	-0.25210900
C	-8.87319700	-1.11269100	-0.75281200
C	-7.99423600	-2.17106800	-0.97996000
C	-0.85004300	3.64098100	2.27733400
N	-0.59316000	4.52132000	2.99656200
H	1.55890300	2.52448900	1.73056000
H	3.30243500	2.13654200	0.04594100
H	0.27372200	1.59856900	-2.96117500
H	-1.47412400	2.03173700	-1.27967700
H	2.64596200	-0.86039300	-1.26976400
H	6.54422300	0.95260900	-1.41383200
H	2.05331700	-3.43535000	1.89684800
H	3.80645700	-3.62828100	2.17540200
H	3.02819800	-2.03791900	2.41589800
H	6.56163300	-3.02988900	3.26265900
H	7.12483300	-1.45580200	2.63389400
H	5.44340000	-1.64055200	3.21738100
H	9.47645800	-0.01725300	0.46529700
H	8.67750200	0.07842200	-1.12698300
H	8.24234100	1.23587500	0.16537300
H	-1.79578800	-2.38356300	-0.01815700
H	-0.95184800	-0.26474800	0.89329700
H	-4.83541900	2.62882900	1.17216300
H	-7.20535300	2.33971300	0.70382800
H	-6.07063400	-4.04890200	-1.32701900
H	-3.67134500	-3.77722800	-0.83839500
H	-9.09297700	0.92296900	-0.07921700
H	-9.93019100	-1.23452000	-0.96857100
H	-8.36608200	-3.11393500	-1.37093300

(a)

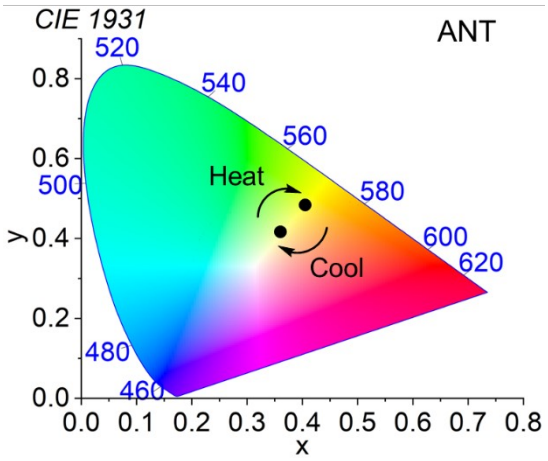

(b)

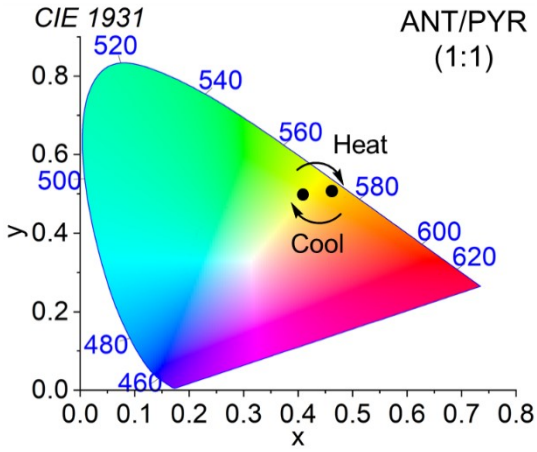

(c)

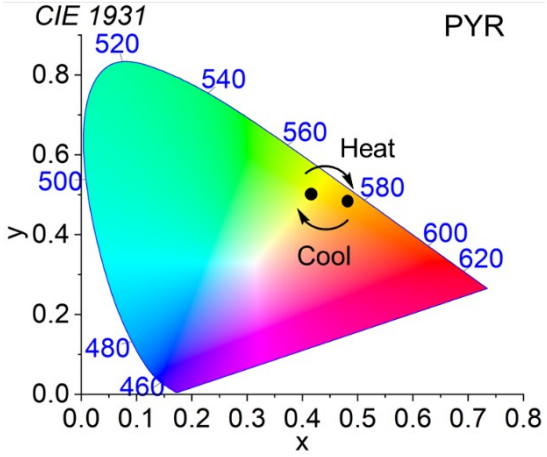

Figure S23. (a) The CIE 1931 chromaticity diagram of **ANT** window exhibits a transition in color coordinates from (0.36, 0.42) to (0.41, 0.48) in water. (b) The CIE 1931 chromaticity diagram of **ANT/PYR (1:1)** window exhibits a transition in color coordinates from (0.41, 0.50) to (0.46, 0.51) in water. (c) The CIE 1931 chromaticity diagram of **PYR** window exhibits a transition in color coordinates from (0.42, 0.50) to (0.48, 0.49) in water.

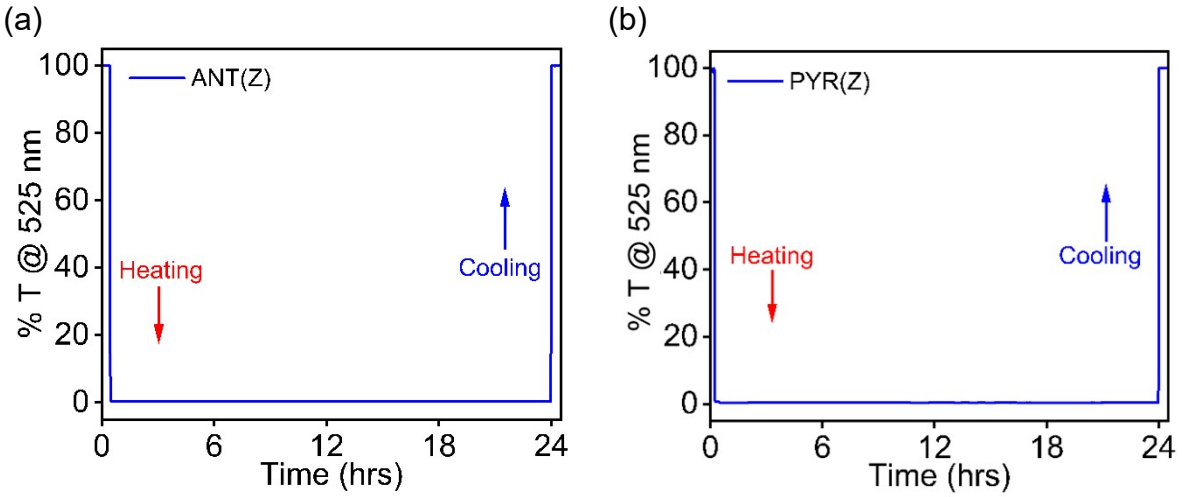

Figure S24. Transmittance stability of (a) **ANT(Z)** and (b) **PYR(Z)** (1 mM) smart windows. There was no detectable degradation in performance for a 24 h period at 60 °C. This experiment was repeated at several cycles for testing the long-term stability of the windows.

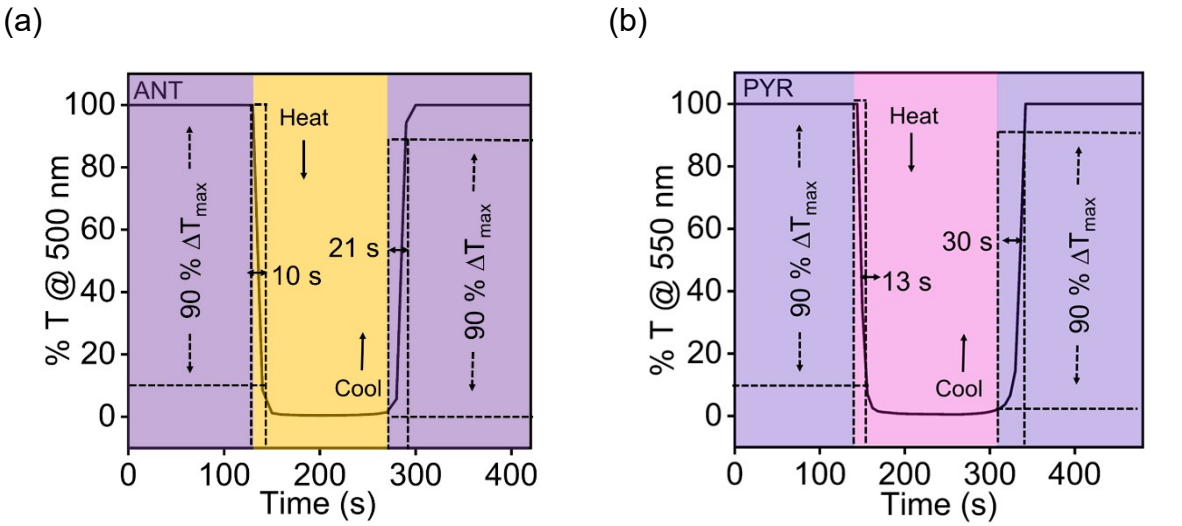

Figure S25. Transmittance switching response of (a) **ANT** and (b) **PYR** (1 mM) for heating and cooling cycles.

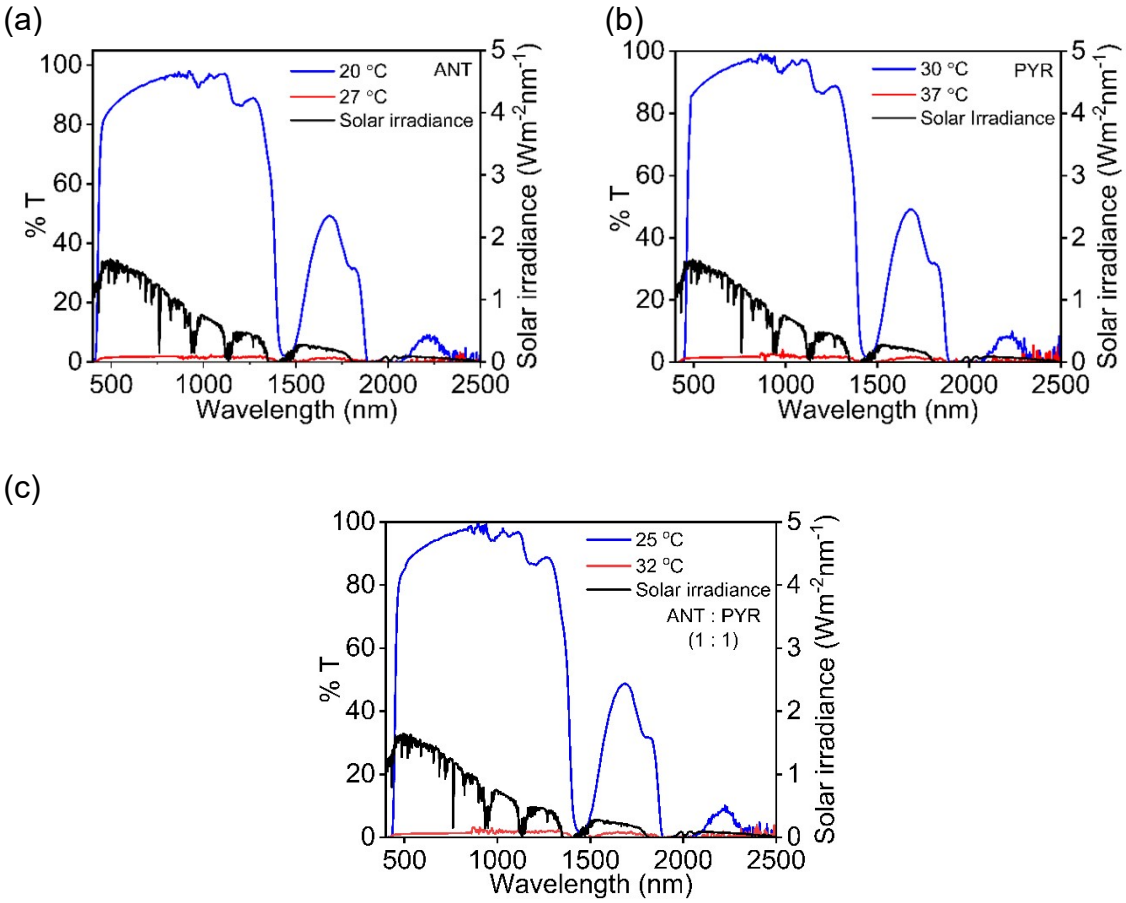

Figure S26. UV-Vis-NIR transmittance spectra (400-2500 nm) of a) **ANT**, b) **ANT: PYR** (1:1) and c) **PYR**, above and below the LCST in comparison with solar radiation spectrum.

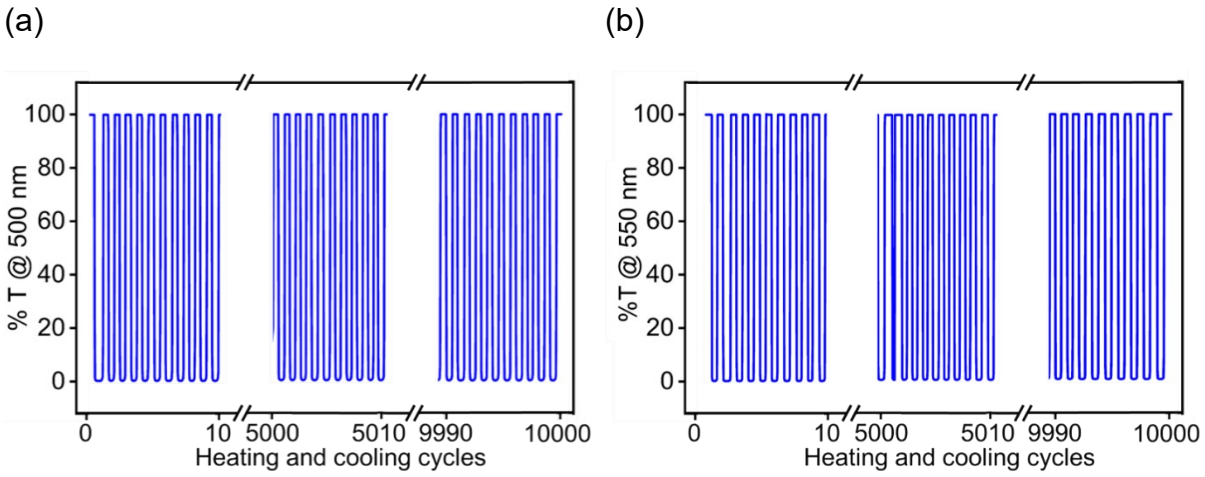

Figure S27. Shelf-life of 10 × 10 cm^2 smart window prototypes of (a) **ANT** and (b) **PYR** for 10,000 heating and cooling cycles.

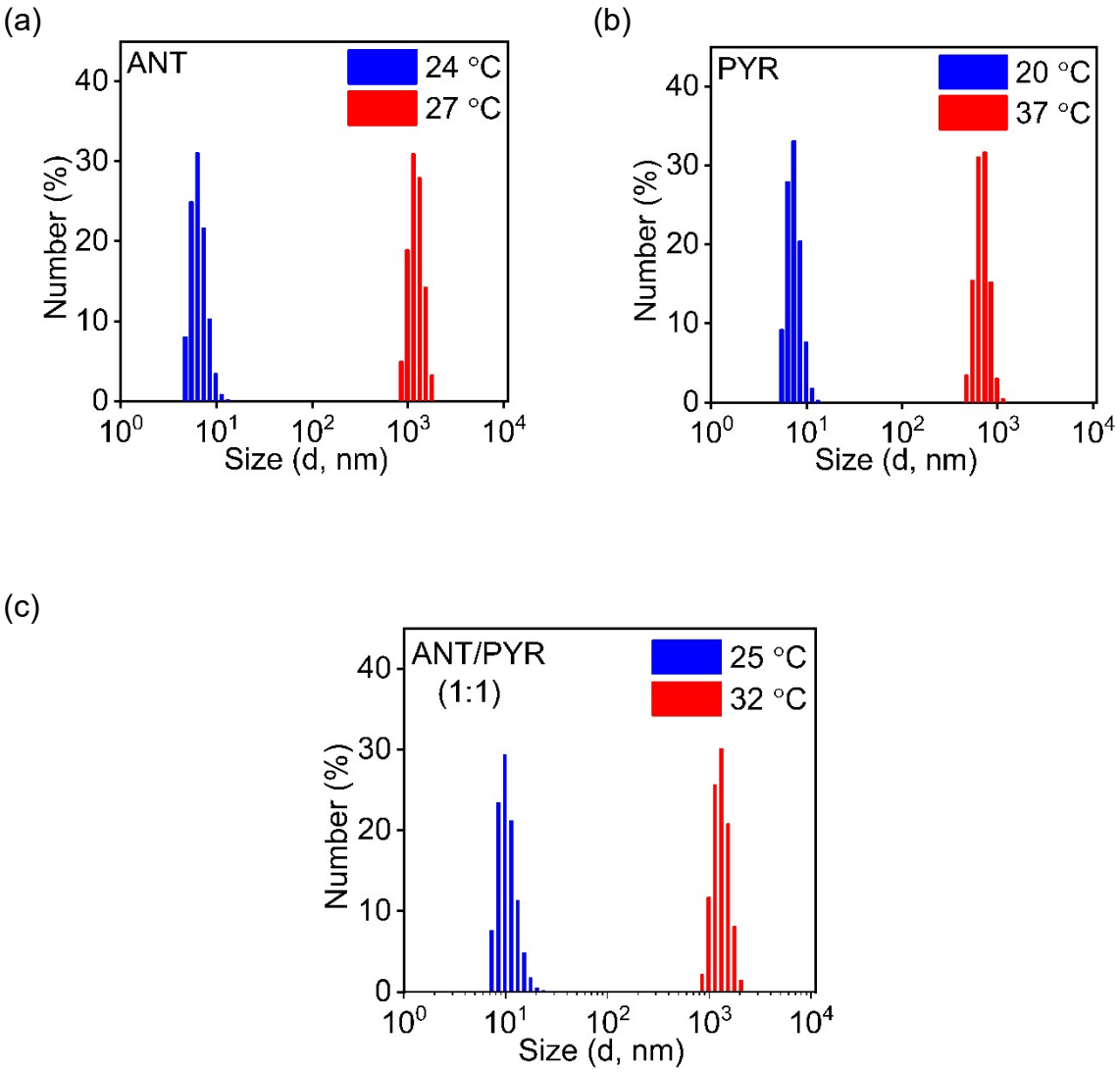

Figure S28. Dynamic light scattering of **ANT**, **PYR**, and **ANT/PYR** (1:1) mixture below and above LCST even after 10,000 heating and cooling cycles, which indicates long-term stability in water.

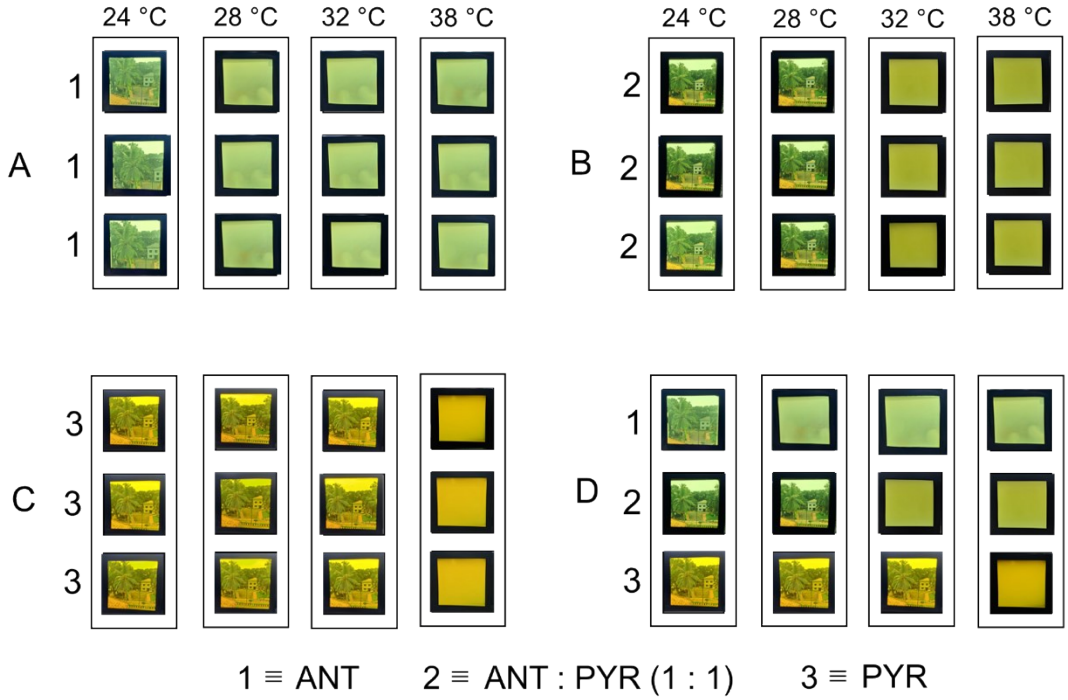

Figure 29. Construction of smart window modules by a mix and match approach, exhibiting autonomous thermal response with variable transparency and color tone. The thermal response of window panels **A**, **B**, **C** and **D** at different temperatures between 24-38 °C are shown.

	A	B	C	D
A	AA	AB	AC	AD
B	BA	BB	BC	BD
C	CA	CB	CC	CD
D	DA	DB	DC	DD

16 possible combinations

	AA	AB	AC	AD
AA	AAAA	AAAB	AAAC	AAAD
AB	ABAA	ABAB	ABAC	ABAD
AC	ACAA	ACAB	ACAC	ACAD
AD	ADAA	ADAB	ADAC	ADAD

16 possible combinations

	BA	BB	BC	BD
BA	BABA	BABB	BABC	BABD
BB	BBBA	BBBB	BBBC	BBBD
BC	BCBA	BCBB	BCBC	BCBD
BD	BDBA	BDBB	BDBC	BDBD

16 possible combinations

	CA	CB	CC	CD
CA	CACA	CACB	CACC	CACD
CB	CBCA	CBCB	CBCC	CBCD
CC	CCCA	CCCB	CCCC	CCCD
CD	CDCA	CDCB	CDCC	CDCD

16 possible combinations

	DA	DB	DC	DD
DA	DADA	DADB	DADC	DADD
DB	DBDA	DBDB	DBDC	DBDD
DC	DCDA	DCDB	DCDC	DCDD
DD	DDDA	DDDB	DDDC	DDDD

16 possible combinations

A 1 1 1 B 2 2 2 C 3 3 3 D 1 2 3

1 ≡ ANT 2 ≡ ANT : PYR (1 : 1) 3 ≡ PYR

Figure S30. Possible combinatorial smart window patterns using modules A, B, C, and D involving a total of 16 direct combinations and other secondary combinations thereof. In this way, large-area glass facades can be constructed with mix-and-match combinations of different modules. A few examples are shown below.

5. Supporting Spectra

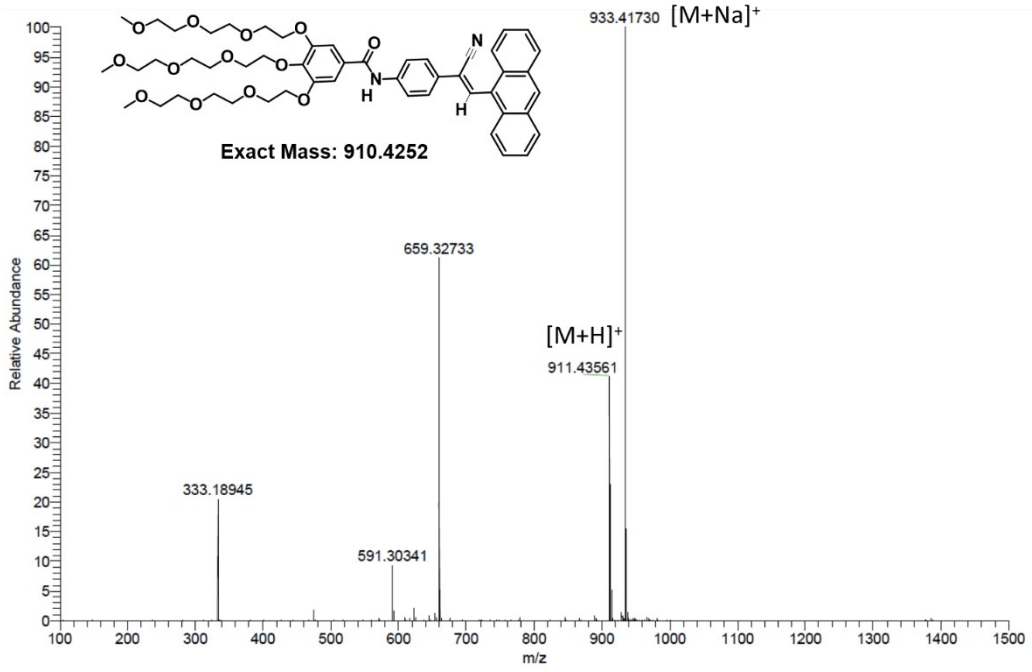

Figure S31. HRMS data of **ANT(Z)**.

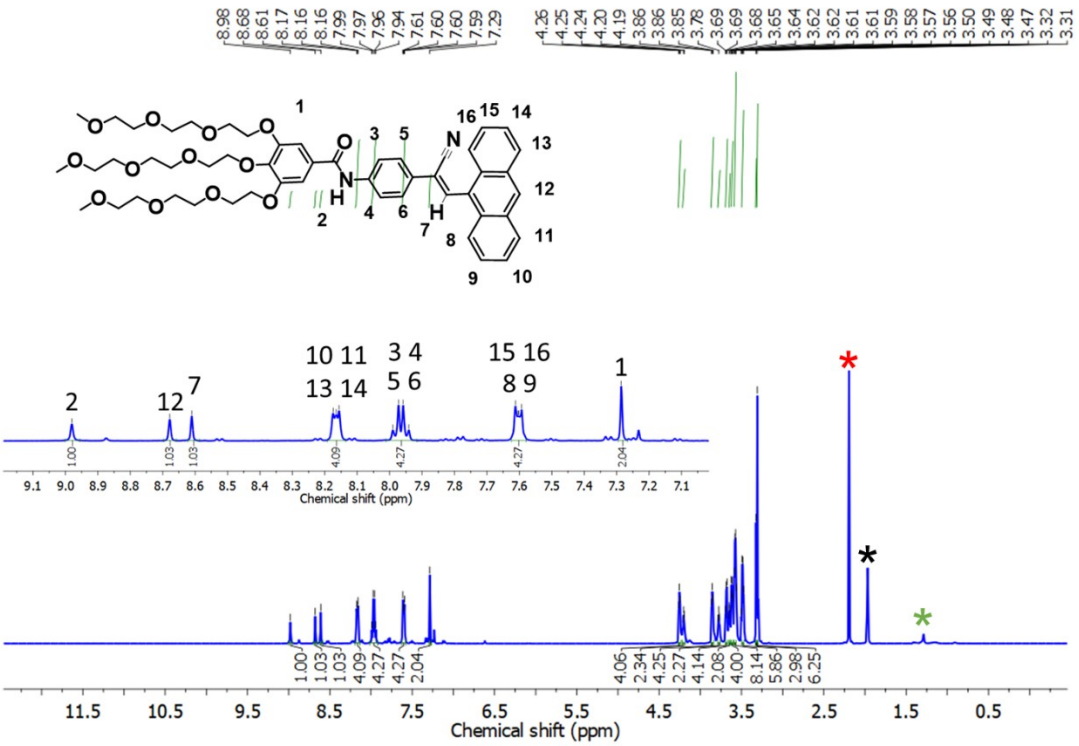

Figure S32. ^{1}H NMR spectrum of **ANT(Z)** (10 mM, CD_3CN, 500 MHz, 25 °C).

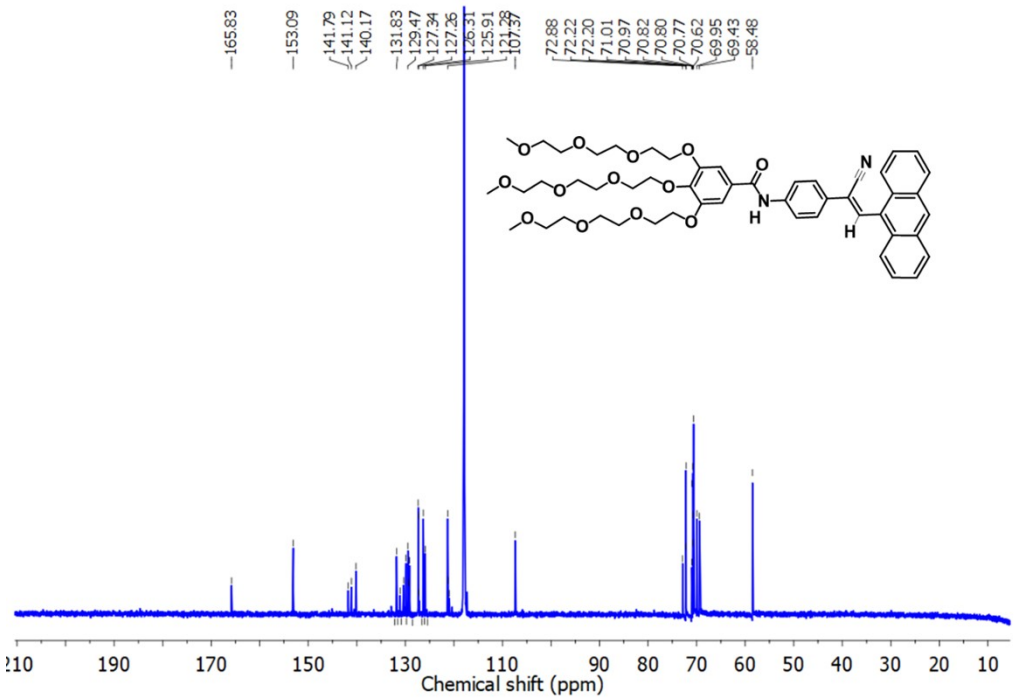

Figure S33. ^{13}C NMR Spectrum of **ANT(Z)** (10 mM, CD_3CN, 125 MHz, 25 °C).

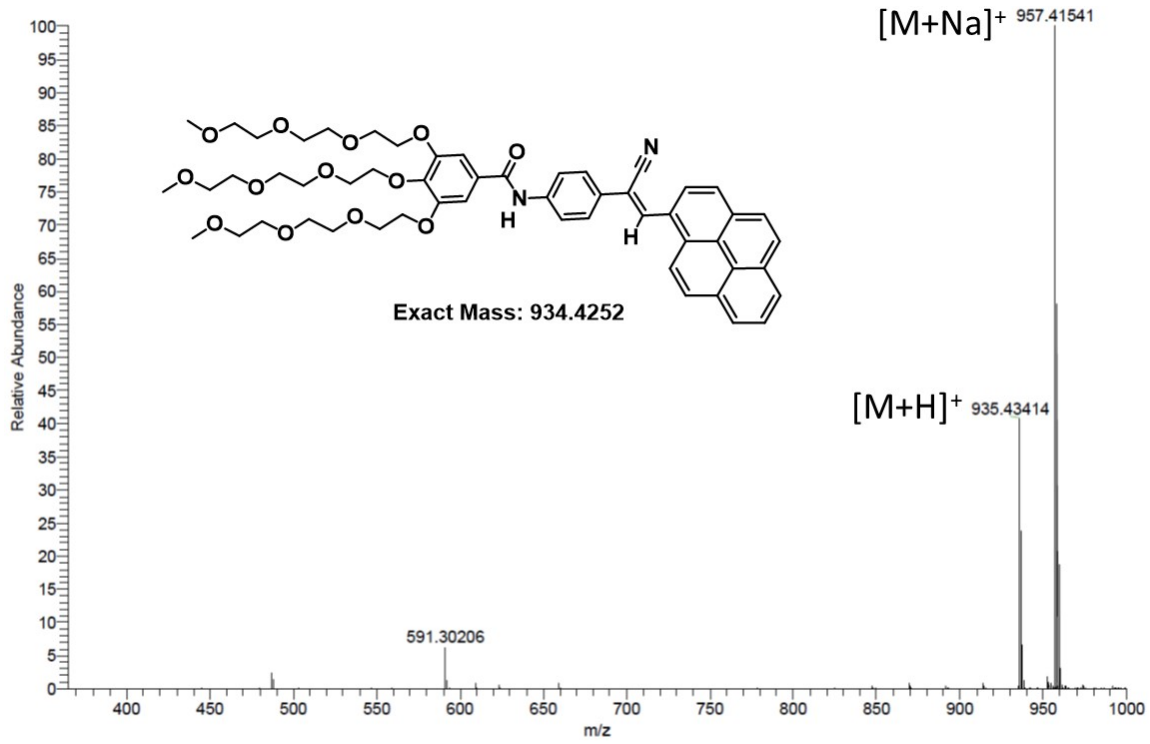

Figure S34. HRMS of **PYR(Z)**.

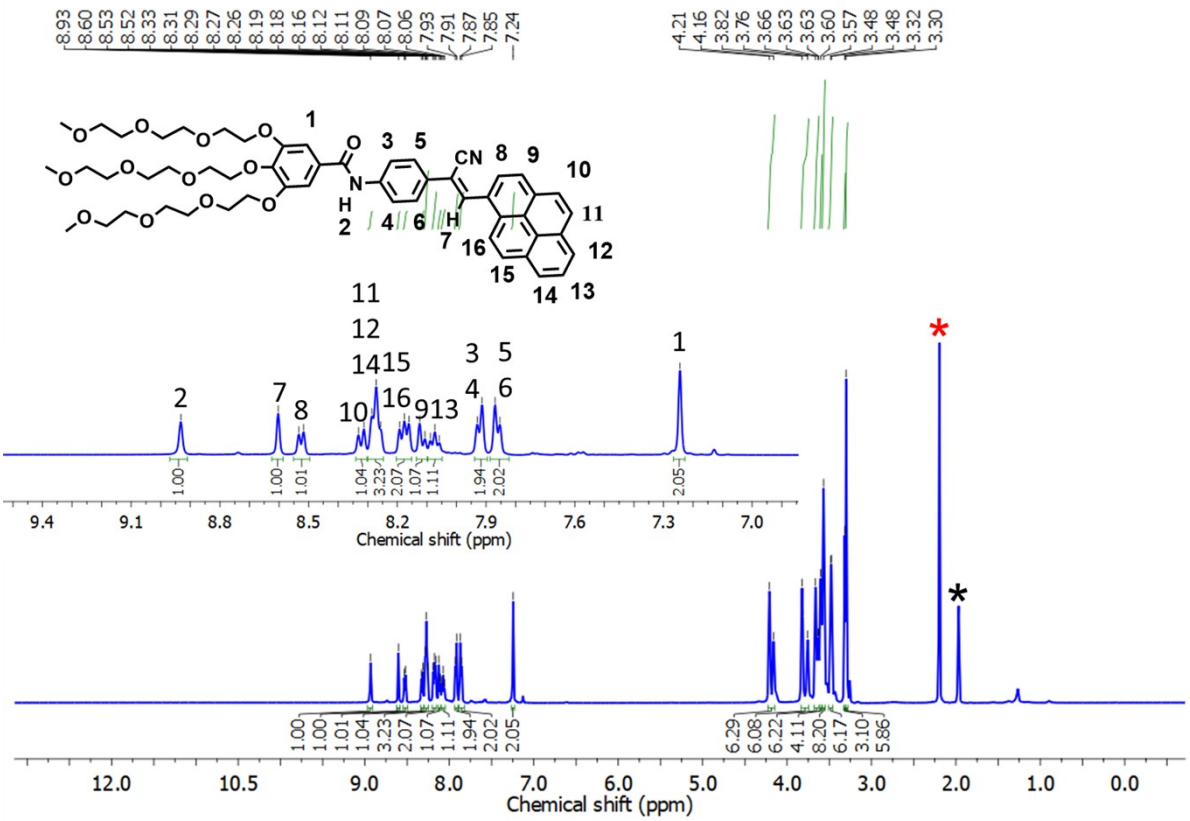

Figure S35. ^{1}H NMR spectrum of **PYR(Z)** (10 mM, CD_3CN, 500 MHz, 25 °C).

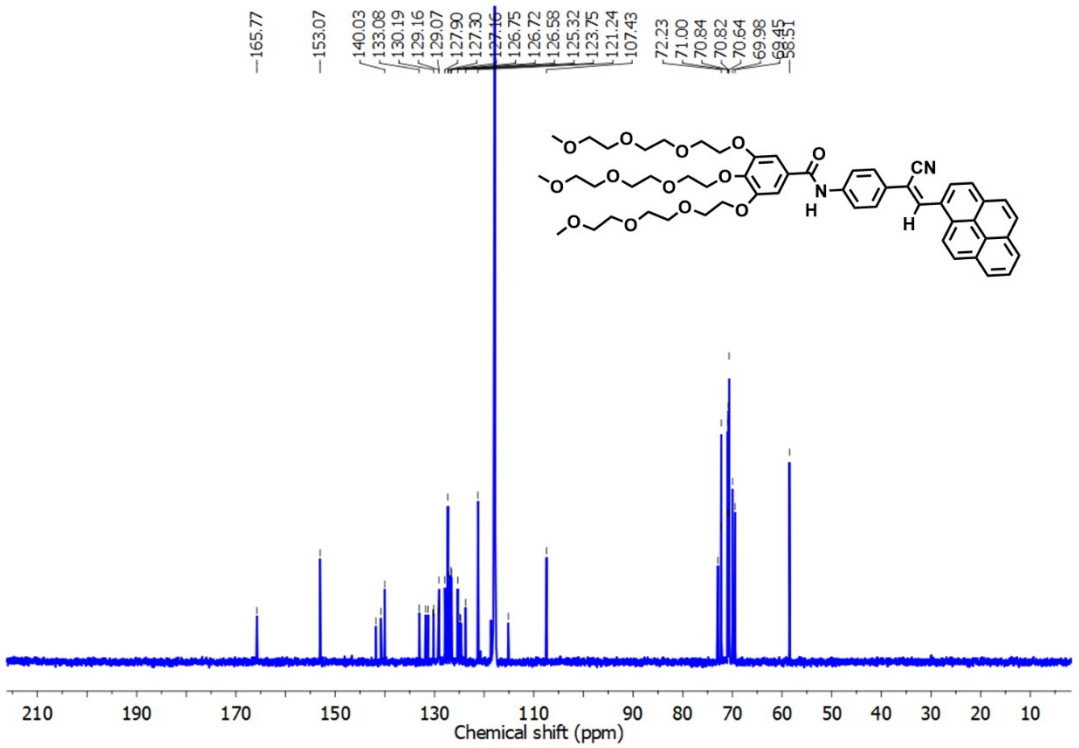

Figure S36. ^{13}C NMR spectrum of **PYR(Z)** (10 mM, CD_3CN, 125 MHz, 25 °C).

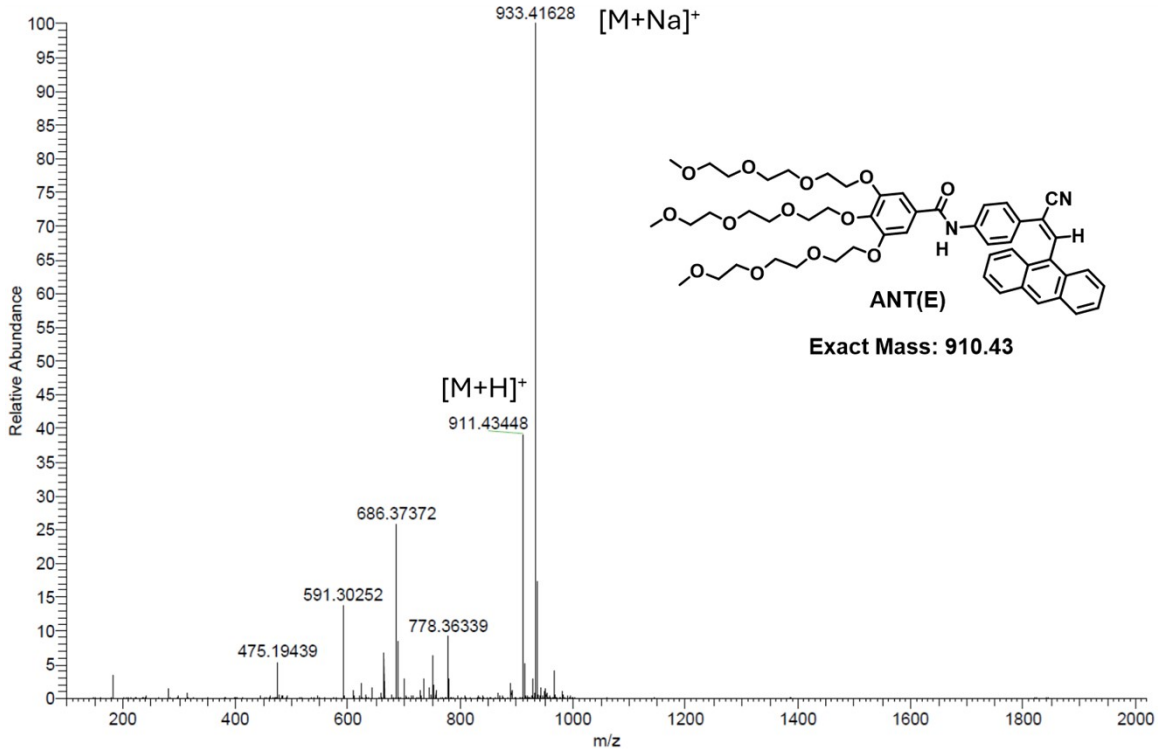

Figure S37. HRMS data of **ANT(E)** after *Z/E*-photoisomerization in water.

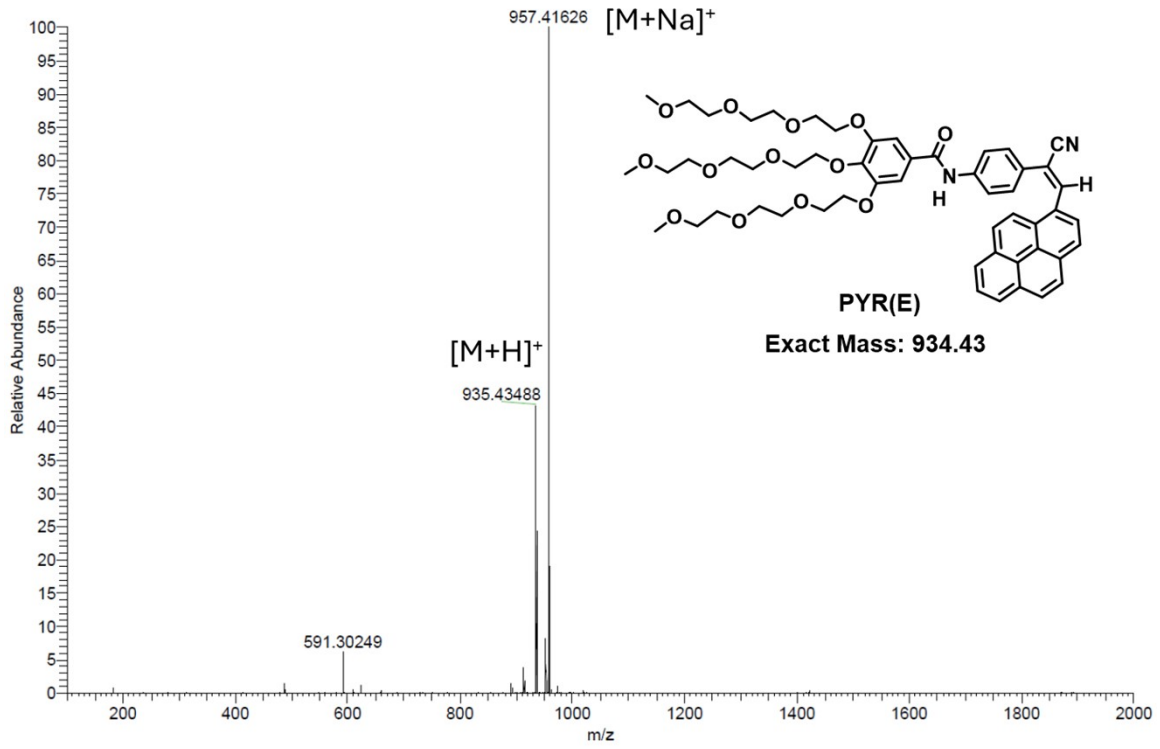

Figure S38. HRMS data of **PYR(E)** after *Z/E*-photoisomerization in water.

6. References

[1] S. Das, D. Patra, S. Shankar, A. Ajayaghosh, *Angew. Chem. Int. Ed.* **2022**, *61*, e202207641.

[2] D. Patra, S. Das, S. Shankar, A. Ajayaghosh, *Adv. Funct. Mater.* **2024**, *34*, 2408014.

[3] F. Xu, S. Crespi, G. Pacella, Y. Fu, M. C. A. Stuart, Q. Zhang, G. Portale, B. L. Feringa, *J. Am. Chem. Soc.* **2022**, *144*, 6019–6027.

[4] R. Lin, P. K. Hashim, S. Sahu, A. S. Amrutha, N. M. Cheruthu, S. Thazhathethil, K. Takahashi, T. Nakamura, T. Kikukawa, N. Tamaoki, *J. Am. Chem. Soc*. **2023**, *145*, 9072–9080.

[5] Y. Zhou, S. Wang, J. Peng, Y. Tan, C. Li, F. Y. C. Boey, Y. Long, *Joule* **2020**, *4*, 2458–2474.

[6] X. H. Li, C. Liu, S. P. Feng, N. X. Fang, *Joule* **2019**, *3*, 290–302.

[7] Y. Cui, Y. Ke, C. Liu, Z. Chen, N. Wang, L. Zhang, Y. Zhou, *Joule* **2018**, 2 (9), 1707-1746.

7. Author Contributions

D.P. has undertaken the synthesis and characterization of the target molecules and performed the experimental work. D.P. and A.G. have designed the experiments, discussed the results, analyzed the data, and co-wrote the manuscript. A.G. was responsible for the overall project concept, direction, coordination, and project funding.